Search of the early O3 LIGO data for continuous gravitational waves from the Cassiopeia A and Vela Jr. supernova remnants

R. Abbott et al. (LIGO Scientific Collaboration and Virgo Collaboration)

Phys. Rev. D **105**, 082005 — Published 28 April 2022

DOI: 10.1103/PhysRevD.105.082005

Search of the Early O3 LIGO Data for Continuous Gravitational Waves from the Cassiopeia A and Vela Jr. Supernova Remnants

LIGO Scientific Collaboration and Virgo Collaboration
(compiled March 21, 2022)

We present directed searches for continuous gravitational waves from the neutron stars in the Cassiopeia A (Cas A) and Vela Jr. supernova remnants. We carry out the searches in the LIGO detector data from the first six months of the third Advanced LIGO and Virgo observing run using the Weave semi-coherent method, which sums matched-filter detection-statistic values over many time segments spanning the observation period. No gravitational wave signal is detected in the search band of 20–976 Hz for assumed source ages greater than 300 years for Cas A and greater than 700 years for Vela Jr. Estimates from simulated continuous wave signals indicate we achieve the most sensitive results to date across the explored parameter space volume, probing to strain magnitudes as low as $\sim 6.3 \times 10^{-26}$ for Cas A and $\sim 5.6 \times 10^{-26}$ for Vela Jr. at frequencies near 166 Hz at 95% efficiency.

I. INTRODUCTION

We report the results of the deepest search to date for continuous gravitational waves from the neutron stars at the centers of the Cassiopeia A (Cas A, G111.7−2.1) [1] and Vela Jr. (G266.2−1.2) [2] supernova remnants. Cas A is just over 300 years old [3, 4], and Vela Jr. may be as young as 700 years old [2]. These extremely young objects have been the target of multiple searches for continuous gravitational waves since 2010 [5–11] because they may retain high rotation frequencies and may possess appreciable non-axisymmetries from their recent births [12–20]. Continuous emission due to unstable r-modes is also possible in such young stars [21–25].

In this search, we analyze the first six months of data from the third observing run (O3a period) of the Advanced Laser Interferometer Gravitational wave Observatory (Advanced LIGO [26, 27]). We achieve significantly improved sensitivity for Vela Jr. with respect to a recent O3a search using a different method [11] and dramatically improved sensitivity for Cas A with respect to previous searches of O1, O2 and O3a LIGO and Virgo data [5–11]. The improvement with respect to similar, previous analyses of O1 data [8, 9] comes largely from the improved detector noise due to a variety of instrument upgrades [28], including a (∼3 db) improvement achieved with quantum squeezing [29].

Given the immense pressure on its nuclear matter, one expects a neutron star to assume a highly spherical shape in the limit of no rotation and, with rotation, to form an axisymmetric oblate spheroid. A number of physical processes can disrupt the symmetry, however, to produce quadrupolar gravitational waves from the stellar rotation. Those processes include crustal distortions from cooling or accretion, buried magnetic field energy and excitation of r-modes. Comprehensive reviews of continuous gravitational wave emission mechanisms from neutron stars can be found in [30, 31]

Central compact objects (CCOs) at the cores of supernova remnants present interesting potential sources, especially those in remnants inferred from their sizes and expansion rates to be young. Both the Cas A and Vela Jr. remnants contain such objects, thought to be young neutron stars. One can derive an estimated age-based upper limit[1] on a CCO's continuous-wave strain amplitude by assuming the star's current rotation frequency is much lower than its rotation frequency at birth and that the star's spin-down since birth has been dominated by gravitational wave energy loss ("gravitar" emission) [32]:

$$h_{\rm age} = (2.3 \times 10^{-24}) \left(\frac{1\,{\rm kpc}}{r}\right) \sqrt{\left(\frac{1000\,{\rm yr}}{\tau}\right)\left(\frac{I_{\rm zz}}{I_0}\right)}, \quad (1)$$

where r is the distance to the source, τ is its age and $I_{\rm zz}$ is the star's moment of inertia about its spin axis, with a fiducial value of $I_0 = 10^{38}$ kg· m^2.

Cas A is perhaps the most promising example of a potential gravitational wave CCO source in a supernova remnant. Its birth aftermath may have been observed by Flamsteed [3] ∼340 years ago in 1680, and the expansion of the visible shell is consistent with that date [4]. Hence Cas A, which is visible in X-rays [33, 34] but shows no pulsations [35], is almost certainly a very young neutron star at a distance of about 3.3 kpc [36, 37]. From equation 1, one finds an age-based strain limit of $\sim 1.2 \times 10^{-24}$, which is readily accessible to LIGO and Virgo detectors in their most sensitive band.

The Vela Jr. CCO is observed in X-rays [38] and is potentially quite close (∼0.2 kpc) and young (690 yr) [2], for which one finds a quite high age-based strain limit of $\sim 1.4 \times 10^{-23}$. Some prior continuous gravitational wave searches have also conservatively assumed a more pessimistic distance (∼1 kpc) and age (5100 yr), based on other measurements [39], for which the age-based strain limit is $\sim 1.0 \times 10^{-24}$, still comparable to that of Cas A.

[1] This strain estimate gives a rough benchmark upper limit on what is possible in an optimistic scenario; its assumption that current rotation frequency is small relative to the star's birth frequency becomes less plausible for the highest frequencies searched in this analysis.

As in the case of Cas A, no pulsations have been detected from Vela Jr. [40, 41].

The remainder of this article is organized as follows: Section II describes the data set used. Section III briefly describes the Weave search program [42] which uses semi-coherent summing of a matched-filter detection statistic known as the $\mathcal{F}$-statistic [43]. Section IV presents the results of the search. Section V discusses the method used to determine 95% sensitivity as an approximation to rigorous upper limits for bands in which all initial search outliers have been followed up with more sensitive but computationally costly methods and dismissed as not credible signals. Section VI concludes with a discussion of the results and prospects for future searches.

II. DATA SETS USED

Advanced LIGO consists of two detectors, one in Hanford, Washington (designated H1), and the other in Livingston, Louisiana (designated L1), separated by a ∼3000-km baseline [26]. Each site hosts one, 4-km-long interferometer inside a vacuum envelope with the primary interferometer optics suspended by a cascaded, quadruple suspension system, affixed beneath an in-series pair of suspended optical tables, in order to isolate them from external disturbances. The interferometer mirrors act as test masses, and the passage of a gravitational wave induces a differential-arm length change which is proportional to the gravitational-wave strain amplitude.

The third Advanced LIGO and Virgo data run (O3) began April 1, 2019 and ended March 27, 2020. The first six months (April 1, 2019 to October 1, 2019), prior to a 1-month commissioning break, is designated as the O3a period. The analysis presented here uses only the O3a data set from the LIGO interferometers. The Virgo data has not been used in this analysis because of an unfavorable tradeoff in computational cost for sensitivity gain, given the interferometer's higher noise level during the O3 run. The systematic error in the amplitude calibration is estimated to be lower than 7% (68% confidence interval) for both LIGO detectors over all frequencies throughout O3a [44].

Prior to searching the O3a data for continuous wave (CW) signals, the quality of the data was assessed and steps taken to mitigate the effects of instrumental artifacts. As in previous Advanced LIGO observing runs [45], instrumental "lines" (sharp peaks in fine-resolution, run-averaged H1 and L1 spectra) are marked, and where possible, their instrumental or environmental sources identified [46]. The resulting database of artifacts proved helpful in eliminating spurious signal candidates emerging from the search; no bands were vetoed *a priori*, however. In general, the number of H1 lines in the O3a data was similar to that observed in the O2 run, while the number of lines for L1 O3a data was substantially reduced.

As discussed in [47], another type of artifact observed in the O3a data for both H1 and L1 were relatively frequent and loud "glitches" (short, high-amplitude instrumental transients) with most of their spectral power lying below ∼500 Hz. To mitigate the effects of these glitches on O3a CW searches for signals below 475 Hz, a simple glitch-gating algorithm was applied [48, 49] to excise the transients from the data.

III. ANALYSIS METHOD

This search relies upon semi-coherent averaging of $\mathcal{F}$-statistic [43] values computed for many short (several-day) segments spanning nearly all of the O3a run period (2019 April 1 15:00 UTC – 2019 October 1 15:00 UTC). Section III A describes the signal model used in the analysis. Section III B describes the mean $\mathcal{F}$-statistic detection statistic at the core of the analysis. Section III C describes the Weave infrastructure for summing individual $\mathcal{F}$-statistic values over the observation period, including the configuration choices for the searches presented in this article. Section III D describes the procedure used to follow up on outliers found in the first stage of the hierarchical search.

A. Signal model and parameter space searched

The signal templates assume a classical model of a spinning neutron star with a time-varying quadrupole moment that produces circularly polarized gravitational radiation along the rotation axis, linearly polarized radiation in the directions perpendicular to the rotation axis and elliptical polarization for the general case. The strain signal model $h(t)$ for the source, as seen by the detector, is assumed to be the following function of time t:

$$h(t) = h_0\big(F_+(t,\alpha_0,\delta_0,\psi)\frac{1+\cos^2(\iota)}{2}\cos(\Phi(t)) + F_\times(t,\alpha_0,\delta_0,\psi)\cos(\iota)\sin(\Phi(t))\big)\ , \qquad (2)$$

In Eq. 2, h_0 is the intrinsic strain amplitude, $\Phi(t)$ is the signal phase, F_+ and $F_\times$ characterize the detector responses to signals with "+" and "×" quadrupolar polarizations [50], and the sky location is described by right ascension α_0 and declination δ_0. In this equation, the star's orientation, which determines the polarization, is parametrized by the inclination angle ι of its spin axis relative to the detector line-of-sight and by the angle ψ of the axis projection on the plane of the sky. The linear polarization case ($\iota = \pi/2$) is the most unfavorable because the gravitational wave flux impinging on the detectors is smallest for an intrinsic strain amplitude h_0, possessing eight times less incident strain power than for circularly polarized waves ($\iota = 0,\ \pi$).

In a rotating triaxial ellipsoid model for a star at distance r spinning at frequency $f_{\rm rot}$ about its (approximate) symmetry axis (z), the amplitude h_0 can be ex-

pressed as

$$h_0 = \frac{4\,\pi^2 G \epsilon I_{zz} f^2}{c^4 r} \quad (3)$$

$$= [1.1\times10^{-24}]\Big[\frac{\epsilon}{10^{-6}}\Big]\Big[\frac{I_{zz}}{I_0}\Big]\Big[\frac{f}{1\,\mathrm{kHz}}\Big]^2\Big[\frac{1\,\mathrm{kpc}}{r}\Big], \quad (4)$$

for which the gravitational radiation is emitted at frequency $f = 2\,f_{\rm rot}$. The equatorial ellipticity ϵ is a useful, dimensionless measure of stellar non-axisymmetry:

$$\epsilon \quad \equiv \quad \frac{|I_{xx} - I_{yy}|}{I_{zz}}. \quad (5)$$

Unstable r-mode emission [21–25] at gravitational wave frequency f (which for this model is $\sim(4/3)f_{\rm rot}$) can be parametrized by a dimensionless amplitude α governing the strain amplitude [51]:

$$h_0 = [3.6\times10^{-23}]\Big[\frac{\alpha}{0.001}\Big]\Big[\frac{f}{1\,\mathrm{kHz}}\Big]^3\Big[\frac{1\,\mathrm{kpc}}{r}\Big]. \quad (6)$$

The phase evolution of the signal is given in the reference frame of the Solar System barycenter (SSB) by the third-order approximation:

$$\Phi(t) = 2\pi\big(f\cdot(t-t_0) + \frac{1}{2}\dot{f}\cdot(t-t_0)^2 + \frac{1}{6}\ddot{f}\cdot(t-t_0)^3\big) + \phi_0\ , \quad (7)$$

where f is the SSB source frequency, $\dot{f}$ is the first frequency derivative (which, when negative, is termed the spin-down), $\ddot{f}$ is the second frequency derivative, t is the SSB time, and the initial phase ϕ_0 is computed relative to reference time t_0 (taken here to be the approximate mid-point of the O3a period: 2019 June 30 15:07:45 UTC – GPS 1245942483). When expressed as a function of the local time of ground-based detectors, Eq. 7 acquires sky-position-dependent Doppler shift terms [43].

In this analysis, we search a band of gravitational wave signal f from 20 to 976 Hz and a frequency derivative $\dot{f}$ range governed by assumed minimum ages τ of each source. Detector noise deteriorates badly below 20 Hz because of ground motion, and in the band around 1000 Hz because of resonant mechanical disturbances. Similar previous searches [5–7] have assumed a power law spin-down: $\dot{f} \propto -f^n$ with braking index n, with n taking on values of 3 for magnetic dipole emission, 5 for GW quadrupole emission (gravitar) and 7 for r-mode emission. For a source that begins at a high frequency and spins down to a much lower present-day frequency with a constant braking index, one expects $\dot{f} \approx \frac{1}{n-1}(f/\tau)$. Allowing for n to range between 2 and 7 because of multiple potential spin-down contributions leads to the search range:

$$-\frac{f}{\tau} \le \dot{f} \le -\frac{1}{6}\frac{f}{\tau}, \quad (8)$$

which has been assumed in several previous searches [5–7]. Here we take a slightly more conservative approach, allowing the upper limit on $\dot{f}$ to reach zero, at modest additional computational cost, while allowing for some time-dependent braking indices and uncertainties in the source's effective age. The range in second frequency derivative $\ddot{f}$ is determined for any frequency f and first derivative $\dot{f}$ by the same relation used in previous searches (governed by the braking index range considered):

$$2\frac{\dot{f}^2}{f} \le \ddot{f} \le 7\frac{\dot{f}^2}{f}. \quad (9)$$

Table I lists the maximum absolute values of $\dot{f}$ and $\ddot{f}$ at the lowest and highest search frequencies, along with the right ascensions and declinations used in the Cas A and Vela Jr. searches.

Source	Cassiopeia A [52]	Vela Jr. [53]
Right ascension	23h 23m 27.85s	8h 52m 1.4s
Declination	+58° 48' 42.8"	–46° 17' 53"
Max. $\lvert\dot{f}\rvert$ (Hz/s) @20 Hz	2.1×10^{-9}	9.1×10^{-10}
Max. $\lvert\dot{f}\rvert$ (Hz/s) @976 Hz	1.0×10^{-7}	4.4×10^{-8}
Max. $\ddot{f}$ (Hz/s^2) @20 Hz	1.6×10^{-18}	2.9×10^{-19}
Max. $\ddot{f}$ (Hz/s^2) @976 Hz	7.6×10^{-17}	1.4×10^{-17}

TABLE I. Sky locations and maximum $|\dot{f}|$, $\ddot{f}$ values used in the Cas A and Vela Jr. searches at the lowest and highest frequencies.

In searching this parameter space, we do not enforce a relation among $(f,\dot{f},\ddot{f})$, which means that for an arbitrary combination, the implied *current* braking index $n_{\rm c}$, defined by $n_{\rm c} \equiv f\ddot{f}/(\dot{f})^2$, may take on arbitrarily large (unphysical) values. For a true power-law behavior over the observation period, the implied third frequency derivative can be written $\dddot{f} = n_{\rm c}(2n_{\rm c}-1)(\dot{f})^2/f^3$. In the initial search and first two stages of outlier follow-up, the third derivative is taken to be zero, which is a good approximation for braking indices below 7 for both sources.

B. The mean $\mathcal{F}$-statistic

This search is based on a semi-coherent average of $\mathcal{F}$-statistic values over many individual intervals of the 6-month observing period. Within each segment of coherence time duration $T_{\rm coh}$, the $\mathcal{F}$-statistic [43] is computed as in previous searches, as a detection statistic proportional to the signal amplitude h_0^2, maximized over h_0, the unknown orientation angles ι and ψ, and the phase constant ϕ_0. In Gaussian noise with no signal present, the value of $2\mathcal{F}$ follows a χ^2 distribution with four degrees of freedom and has an expectation value of four. The presence of a signal leads to a non-central χ^2 distribution with a non-centrality parameter proportional to

$h_0^2 \cdot T_{\rm coh}$ and inversely proportional to the average power spectral density of the detector noise. The non-centrality parameter also depends on the source's orientation and sky location, and on the orientations and locations of the LIGO interferometers [43].

We compute a semi-coherent mean $\mathcal{F}$-statistic we call $2\bar{\mathcal{F}}$ from the average value of $2\mathcal{F}$ over the $N_{\rm seg}$ segments into which the observing period is divided:

$$2\bar{\mathcal{F}} = \frac{1}{N_{\rm seg}} \sum_{i=1}^{N_{\rm seg}} 2\mathcal{F}_i. \tag{10}$$

In the absence of signal, this detection statistic too has an expectation value of four, but has the underlying shape of a χ^2 distribution with $4N_{\rm seg}$ degrees of freedom with a (rescaled) standard deviation of $\sqrt{8/N_{\rm seg}}$. The presence of a signal leads to an offset in the mean that is approximately the same as the non-centrality parameter above, for a fixed $T_{\rm coh}$.

C. The Weave infrastructure

The Weave software infrastructure provides a systematic approach to covering the parameter space volume in a templated search to ensure acceptable loss of signal-to-noise ratio (SNR) for true signals lying between template points [42]. The Weave program combines together recent developments in template placement to use an optimal parameter-space metric [54, 55] and optimal template lattices [56]. The package is versatile enough to be used in all-sky searches for unknown sources. Here we use a simpler configuration applicable to well localized sources, such as Cas A and Vela Jr.

In brief, a template grid in the parameter space is created for each time segment, a grid that is appropriate to computing the $\mathcal{F}$-statistic[2] for a coherence time $T_{\rm coh}$ equal to the total observation period $T_{\rm obs}$ divided by $N_{\rm seg}$. The spacing of the grid points in $(f, \dot{f}, \ddot{f})$ is set according to a metric [54, 55] that ensures a worst-case maximum mismatch $m_{\rm coh}$ defined by the fractional loss in $2\mathcal{F}$ value due to a true signal not coinciding with a search template.

Separately, a much finer grid is defined for the full observation period with respect to the midpoint of the observation period, one with its own mismatch parameter $m_{\rm semi-coh}$, analogous to $m_{\rm coh}$, but defined to be the average of the coherent mismatch values over all segments [55]. It choice is set empirically in a tradeoff between sensitivity and computational cost. The Weave package creates at initialization a mapping between each point in the semi-coherent template grid and a nearest corresponding point in each of the separate, coarser segment grids, accounting for frequency evolution. The semi-coherent detection statistic $2\bar{\mathcal{F}}$ is constructed for each semi-coherent template from this mapping [42].

For the Cas A and Vela Jr. searches presented here, a simulation study was carried out to evaluate tradeoffs in achievable sensitivity for a small but diverse set of segment length choices ($T_{\rm coh}$) and mismatch parameters $m_{\rm coh}$ and $m_{\rm semi-coh}$, with a goal of staying within a maximum computational cost of 3×10^6 CPU core hours for the two searches combined, including for outlier follow-up ($\sim$10%). Searching over only f and $\dot{f}$ was also explored, but yielded poorer sensitivity. In the end, we chose the Weave configuration parameters shown in Table II.

Search jobs are carried out in 0.1-Hz bands of f, with further divisions in $\dot{f}$, as needed, to keep each job's computational duration between approximately 6 and 12 hours, for practical reasons. Tables III-IV show the number of $\dot{f}$ divisions *vs.* frequency band for the two searches.

D. Outlier follow-up

Each individual job returns the $(f,\dot{f},\ddot{f})$ values of the 1000 templates ("top-list") with the largest ("loudest") $2\bar{\mathcal{F}}$ values. For 0.1-Hz bands with $N_{\dot{f}}$ divisions in the $\dot{f}$ range, there are $N_{\dot{f}} \times 1000$ values returned. Outlier templates to be followed up are those in these top-lists exceeding a frequency-dependent threshold $2\bar{\mathcal{F}}_{\rm thresh}(f)$ which rises slowly with f as the number of distinct templates searched grows, thereby increasing the statistical trials factor. A nominal threshold is set based on the signal-free χ^2 distribution with four degrees of freedom per segment such that the expectation value of outliers is one per 1-Hz band in Gaussian noise, given the empirically obtained trials factor. Using the template counts from the Weave configuration yields an empirical fitted function $2\bar{\mathcal{F}}_{\rm thresh}(f) = 2\bar{\mathcal{F}}_0 f^a$, where the parameters $2\bar{\mathcal{F}}_0$ and a are listed in Table V.

In practice, non-Gaussian artifacts lead to much higher outlier counts in particular bands contaminated by instrumental line sources (Sect. II). In some cases strong instrumental lines can lead to more than 1000 templates from a single job that exceed the threshold for a particular 0.1-Hz band and range of $\dot{f}$ searched. We refer to those cases as "saturated" since potentially interesting templates may be suppressed by the top-list cap. Each of those cases is examined manually to assess instrumental contamination. Where such contamination is confirmed, those bands are marked and excluded from those in which we quote strain sensitivities. The appendix lists these 0.1-Hz bands.

For non-saturated sub-ranges of individual 0.1-Hz bands, outliers exceeding the threshold $2\bar{\mathcal{F}}_{\rm thresh}(f)$ are followed up in a sequential procedure where at each step, the coherence time $T_{\rm coh}$ is doubled (and hence the number

[2] To understand better the effects of instrumental line artifacts, in this initial exploration of the O3 data with the Weave method, a "pure" $\mathcal{F}$-statistic was used rather than the Bayesian-motivated $\mathcal{F}^{+\rm veto}$-statistic [57, 58], in which the $\mathcal{F}$-statistic value is suppressed by the presence of line artifacts in one detector, but not in the other.

Parameter	Cas A	Vela Jr.
Coherent mismatch $m_{\rm coh}$	0.1	0.1
Semi-coherent mismatch $m_{\rm semi-coh}$	0.2	0.2
Coherence time (number of segments) for initial search	5.0 days (36)	7.5 days (24)
Coherence time (number of segments) for 1st follow-up	10.0 days (18)	15.0 days (12)
Coherence time (number of segments) for 2nd follow-up	20.0 days (9)	30.0 days (6)
Coherence time (number of segments) for 3rd follow-up	45.0 days (4)	60.0 days (3)

TABLE II. WEAVE configuration parameters used for the Cas A and Vela Jr. searches.

Frequency band	Number of $\dot{f}$ sub-ranges
20–151 Hz	1
151–251 Hz	5
251–301 Hz	10
301–401 Hz	20
401–501 Hz	30
501–555 Hz	35
551–651 Hz	45
651–701 Hz	55
701–801 Hz	85
801–926 Hz	105
926–976 Hz	130

TABLE III. Numbers of $\dot{f}$ sub-ranges into which the initial Cas A search jobs (0.1-Hz sub-bands) are divided for different frequency search bands, in order to maintain job durations between about 6 and 12 computational hours. Each sub-band is subject to a 1000-candidate top-list.

Frequency band	Number of $\dot{f}$ sub-ranges
20–201 Hz	1
201–401 Hz	5
401–501 Hz	10
501–701 Hz	20
701–901 Hz	40
901–976 Hz	60

TABLE IV. Numbers of $\dot{f}$ sub-ranges into which the initial Vela Jr. search jobs (0.1-Hz sub-bands) are divided for different frequency search bands, in order to maintain job durations between about 6 and 12 computational hours. Each sub-band is subject to a 1000-candidate top-list.

Source	$2\bar{\mathcal{F}}_0$	a	$2\bar{\mathcal{F}}_{\rm thresh}(20\ {\rm Hz})$	$2\bar{\mathcal{F}}_{\rm thresh}(976\ {\rm Hz})$
Cassiopeia A	7.64	0.0227	8.18	8.93
Vela Jr.	8.48	0.027	9.19	10.21

TABLE V. Parameters defining the analytic threshold function $2\bar{\mathcal{F}}_{\rm thresh}(f) = 2\bar{\mathcal{F}}_0 f^a$ applied to the $2\bar{\mathcal{F}}$ detection statistic to define initial outliers for follow-up. Threshold values evaluated for $f = 20$ and 976 Hz are also shown.

of segments $N_{\rm seg}$ is halved). Because the non-centrality parameter for the mean $2\bar{\mathcal{F}}$ detection statistic scales approximately linearly with $T_{\rm coh}$, one expects a nominal doubling of the *excess* mean $2\bar{\mathcal{F}}$ defined by $2\bar{\mathcal{F}} - 4$.

To be conservative and guided by simulations, we require outliers passing a follow-up stage to display an increase of 60–70% in excess mean $2\bar{\mathcal{F}}$ with respect to the previous stage, depending on source and follow-up stage. Table VI lists the required increaes, which are lower for Cas A than for Vela Jr. in the first follow-up stages because its younger age leads to higher possible 3rd frequency derivatives which are not searched over in those stages. The simulated signals used to guide these choices are nominally detectable but not loud, having strain amplitudes ranging from ∼1.1–1.5 times the estimated strain amplitude $h_{\rm sens}^{95\%}$ for which the $2\bar{\mathcal{F}}_{\rm thresh}(f)$ threshold yields 95% efficiency (see Sect. V). The required increases in $2\bar{\mathcal{F}}$ leads to an losses in overall signal efficiency below ∼2% for braking indices below 7. For each follow-up stage, the search space around each outlier's values of f, $\dot{f}$ and $\ddot{f}$ was chosen to be three times (in all dimensions) the template step sizes used in the previous stage. In the third stage, the range of $\dddot{f}$ searches is from zero to twice the implied value of the 2nd-round survivor, assuming a power law spindown during the observation period. All of these follow-up requirements and resulting efficiencies were evaluated by end-to-end software injections.

In the first stage of follow-up, all outliers above threshold are evaluated. In that initial stage, which more finely samples the parameter space, multiple outliers may survive the next threshold requirement. In successive stages, only the loudest survivor corresponding to the outlier being evaluated is passed to the next stage of follow-up. Pursuing only the loudest survivor per initial outlier preserves high detection efficiency for a true signal while

Source	Round 1 increase	Round 2 increase	Round 3 increase
Cassiopeia A	65%	60%	70%
Vela Jr.	70%	70%	70%

TABLE VI. Required increases in excess mean $2\bar{\mathcal{F}}$ in each stage of outlier follow-up. The third frequency derivative $\ddot{f}$ is taken to be zero in the first two stages, but explicitly searched over in the third follow-up stage.

reducing computational cost from following up multiple candidate templates contaminated by the same instrumental disturbance.

IV. SEARCH RESULTS

The search described above was carried out on the O3a data for the Cas A and Vela Jr. sources. For Cas A (Vela Jr.), there were $\sim 2 \times 10^5$ ($\sim 1 \times 10^5$) outliers above threshold from the initial search in bands that were not excluded from consideration by severe instrumental artifacts. These outliers were all followed up individually with a narrowed search and a doubling of the coherence time. An outlier was considered to survive follow-up if the loudest candidate template from its follow-up displayed an increase of 70% or more in excess $2\bar{\mathcal{F}}$ with respect to the original outlier's excess $2\bar{\mathcal{F}}$. This criterion led to $\mathrm{O}(1.5 \times 10^4)$ survivors for each source. That loudest surviving template then served as a seed for a second round of follow-up using another doubling of coherence time. Once again, survivors of the round were defined by another increase by at least 70% in excess $2\bar{\mathcal{F}}$ with respect to the seed template, leading to $\sim 10^3$ ($\sim 2 \times 10^3$) 2nd-round survivors for Cas A (Vela Jr.).

Survivors of this second round of follow-up were all clustered and the loudest template visually inspected, to assess instrumental line contamination. Clustering was carried out in frequency using simple grouping of any survivor template within 0.01 Hz of another survivor template. Tables VII–VIII list the parameters of the single loudest outlier in each cluster. In nearly every band a loud instrumental artifact was apparent. To identify these contaminations, we construct so-called "strain histograms" in which the summed power over the observation period from a simulation of the nominal signal candidate is superposed on a background estimate of the noise estimated via interpolation between neighboring frequency bands. For computational efficiency, the summed power is approximated via a histogram of rescaled integer counts from each 30-minute digital Fourier transform used in the search. Except for signal templates with high-magnitude spin-downs, the histograms typically display at least one "horn" (narrow peak) from an interval during the 6-month O3a period when the orbitally modulated frequency is relatively stationary.

We discard outliers for which the signal template's shape either aligns with a spectral artifact known to be instrumental, or else appears much louder in one detector than the other which is inconsistent with time-averaged antenna pattern sensitivities. Figures 1-2 show example strain histograms for Cas A and Vela Jr. outliers that are both heavily contaminated by an H1 spectral line at 48.000 Hz. Figures 1-2 also show graphs of the outlier templates' detector-frame frequencies *vs.* time during the O3a period, illustrating periods of relatively stationary frequency. For these templates there is an approximate cancellation between the source intrinsic spin-down and an apparent spin-up of frequency caused by the Earth's general acceleration toward the direction of Cas A early in O3a and toward the direction of Vela Jr. after the midpoint of O3a. Since source frequencies are defined by the midpoint of the O3a run, the Cas A (Vela Jr.) template frequencies susceptible to this stationarity generally lie below (above) the detector-frame frequency of the line artifact contaminating the template recovery.

A small number of outlier clusters for which a sharp line contamination is not the obvious cause were examined further. The Cas A outliers at 52.8052 Hz and 145.3899 Hz (in a saturated sub-band) are due to contamination from loud "hardware injections." These injections are simulated signals imposed via modulated forces on interferometer mirrors during data taking. See [47, 60] and [61] for more details on the hardware injections carried out during the O3a run. For these outliers, the contaminations arise from injection "Inj5" and "Inj6" (see Table IV of [47]), which both simulate CW sources near the sky location of Cas A. The Inj5 injection is loud enough to show up as a Vela Jr. outlier too.

The 11 Cas A outliers in Table VII and 3 Vela Jr. outliers in Table VIII that are marked with asterisks occur in spectral bands in which instrumental lines are plentiful, but for which no clearcut artifact allows immediate discarding of the outliers. For these outliers, a third round of follow-up was carried out, with a third increase in coherence time: from 20 to 45 days (from 9 to 4 segments) for Cas A and from 30 to 60 days (from 6 to 3 segments) for Vela Jr.. Because of the lengths of these coherently analyzed segments, these follow-ups included a search over the third frequency derivative $\ddot{f}$. Simulations indicate that a 70% increase in excess $2\bar{\mathcal{F}}$ is a conservative requirement, including for unphysically large braking indices, given that preceding follow-up stages do not allow for a non-zero $\ddot{f}$. None of these outliers satisfies this 70% requirement, and none has a braking index in the range 1–7.

Figures 3-4 show the Cas A and Vela Jr. outlier and survivor counts in 1-Hz bands for the multiple stages of analysis, starting with outliers exceeding the threshold $2\bar{\mathcal{F}}_{\mathrm{thresh}}(f)$ and proceeding to those surviving the successive requirements that the excess $2\bar{\mathcal{F}}$ increase by 70% each round of follow-up. Saturated sub-bands listed in the appendix are shaded.

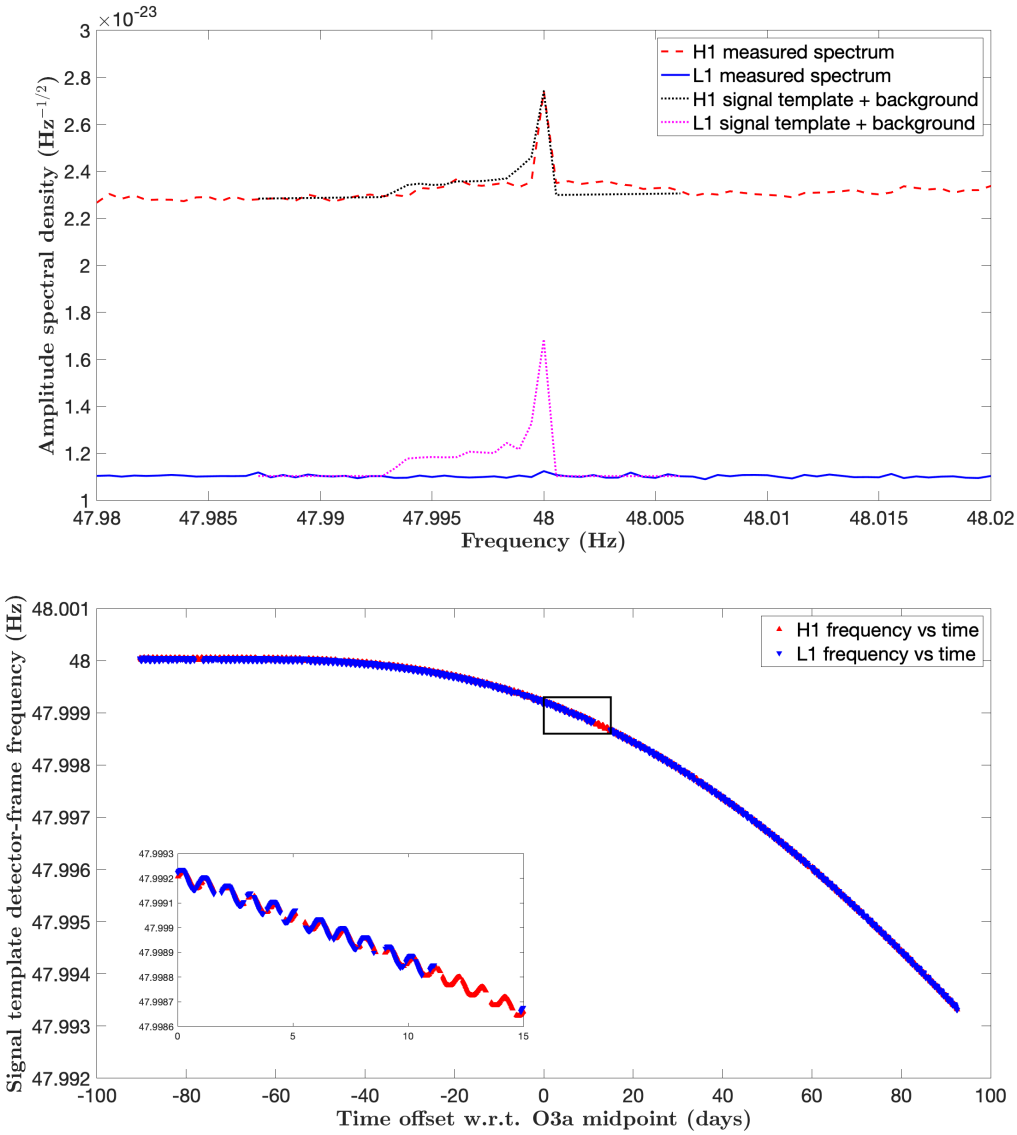

FIG. 1. *Upper panel:* Example of "strain histogram" graph for Cas A used in vetoing outliers for which instrumental contamination is apparent. The curves show the O3a-run-averaged H1 (red dashed) and L1 (blue solid) amplitude spectral densities in a narrow band containing an artifact at 48.000 Hz. The dotted curves show histograms of expected strain excess from H1 (black) and L1 (magenta) signal templates added to smooth backgrounds interpolated from neighboring frequency bands. In this depiction, the strain amplitude of the signal template has been magnified by an arbitrary factor large enough to make the signal's structure clear. The large excess power in the H1 data, not seen in the L1 data, despite comparable strain sensitivities and comparable sidereal-averaged antenna pattern sensitivities, excludes an astrophysical source for the H1 artifact. The fact that the artifact aligns in frequency with the putative signal's template peak in power confirms contamination of the outlier from an instrumental source. In addition, the line at precisely an integer frequency is part of a known instrumental spectral comb in the O3a H1 data. *Lower panel:* Graph of the corresponding template signal frequencies *vs.* time during O3a in the H1 and L1 interferometer reference frames, in which frequency points are plotted for only those 30-minute segments used in the analysis. One sees a relatively stationary period early in the run for Cas A. The inset box shows a magnification of the frequency *vs.* time graph for a 15-day period starting at the midpoint of the O3a interval, one that includes a multi-day period during which no data was collected from the L1 interferometer because Hurricane Barry disrupted observatory operations. The magnification makes more clear the diurnal modulation of the reference-frame frequency by the Earth's rotation about its axis, with slightly larger modulations seen for the lower-latitude L1 interferometer than for H1 (color online).

f (Hz)	$\dot{f}$ (nHz/s)	$\ddot{f}$ (aHz/s^2)	f (Hz)	$\dot{f}$ (nHz/s)	$\ddot{f}$ (aHz/s^2)	f (Hz)	$\dot{f}$ (nHz/s)	$\ddot{f}$ (aHz/s^2)	f (Hz)	$\dot{f}$ (nHz/s)	$\ddot{f}$ (aHz/s^2)
22.2597	−0.18	85.6	64.8765	−0.54	24.5	515.1569	−1.86	20.2	630.3393	−65.77	−9.6
22.6684	−0.41	50.4	64.9955	−0.71	3.7	520.4822	−3.13	4.3	630.3606	−66.06	30.6
24.9982	−0.27	1.5	67.9953	−0.74	4.0	*520.6814	−2.86	−28.5	630.3788	−64.06	−4.5
28.0001	−0.13	1.7	73.9948	−0.82	2.4	*520.7275	−10.13	47.5	630.6003	−33.38	20.4
29.7984	−0.33	0.9	74.1949	−0.81	3.2	*520.7408	−12.02	7.6	630.7146	−56.47	13.4
30.1978	−0.38	−5.5	74.9948	−0.81	4.9	*521.4661	−0.62	−6.4	638.3140	−4.82	0.8
30.8993	−0.11	65.0	79.9947	−0.78	19.6	*521.4895	−4.25	17.9	640.4433	−7.18	−63.6
30.9979	−0.32	4.1	84.3942	−0.91	4.0	521.5134	−7.75	−27.4	799.9366	−8.06	51.6
*31.3903	−0.33	2.4	90.8932	−1.11	−12.7	521.5494	−5.77	21.0	898.7328	−18.60	135.3
32.4983	−0.10	57.7	92.4500	−0.21	50.1	*522.1882	−4.01	1.0	898.9294	−46.32	36.2
33.8982	−0.10	64.0	107.2843	−0.33	79.8	527.3181	−5.26	−10.7	898.9575	−41.81	58.2
35.8831	−0.13	72.6	107.4488	−1.15	2.3	528.5258	−3.66	−5.6	898.9840	−34.74	56.2
37.9276	−0.43	−28.1	119.9910	−1.30	6.1	*533.4444	−5.94	−0.1	898.9993	−32.69	58.5
37.9974	−0.41	2.4	301.9999	−28.76	113.5	599.6389	−53.61	32.4	899.1333	−41.93	110.5
38.8732	−0.09	70.0	316.7777	−3.49	12.2	599.9509	−6.48	0.7	899.1675	−30.36	107.9
40.7971	−0.45	1.5	333.3861	−27.40	0.2	604.7859	−56.67	11.9	899.1826	−24.69	−31.6
42.3823	−1.10	73.6	348.5643	−5.62	−49.1	606.4225	−62.43	30.0	899.2032	−12.52	17.5
43.3672	−1.14	−30.9	368.5754	−3.85	32.5	606.7767	−49.63	9.0	906.6986	−17.85	120.9
44.3524	−1.18	1.8	485.2598	−9.74	13.7	606.8898	−52.72	33.0	909.7752	−49.35	67.2
45.3311	−0.17	66.3	485.2772	−4.83	2.7	612.2997	−50.45	34.4	910.1130	−6.43	−10.9
46.5430	−0.06	30.6	*487.9915	−4.36	11.2	612.4531	−54.58	38.2	918.6993	−15.63	7.8
46.7866	−4.35	9.6	*489.5465	−12.82	33.2	615.0071	−57.32	42.1	918.7291	−27.25	15.9
51.6816	−0.15	97.0	493.7602	−0.14	104.8	615.0244	−59.39	19.3	918.8026	−1.51	1.9
52.8052	−0.85	9.3	494.7315	−2.90	5.3	615.0373	−61.00	79.0	918.8164	−24.96	18.9
54.7779	−0.28	−74.9	495.0989	−0.03	−4.9	615.0512	−60.78	74.8	922.5653	−18.33	7.3
54.8952	−0.55	11.6	501.1989	−47.07	31.7	629.8061	−10.30	−9.6	922.5866	−13.49	−34.6
57.0006	−3.78	−20.8	504.7002	−3.39	−1.6	629.8195	−9.25	2.2	*945.1703	−19.85	20.8
60.7084	−0.09	8.9	506.4994	−28.63	20.5	629.8375	−15.47	16.1	945.1870	−14.94	−0.3
60.8843	−0.36	59.6	511.9005	−35.97	−92.9	630.3149	−64.10	−1.9	945.5873	−13.65	−76.8

TABLE VII. Frequency parameters for the loudest Cas A outlier in each cluster that survived round 2 follow-up. Outliers marked with asterisks were followed up with a third round.

We conclude that there is no significant evidence in this analysis for a continuous wave signal from the compact objects at the centers of the Cas A or Vela Jr. supernova remnants.

V. ESTIMATING SEARCH SENSITIVITY

Given the absence of a detection, we quote 95%-efficiency amplitude sensitivities $h_{\rm sens}^{95\%}$ for every band in which there were no outliers above the initial $2\bar{\mathcal{F}}$ threshold or for which every outlier was followed up and found not to be a credible signal. Those bands (listed in the appendix) with at least one $\dot{f}$ interval exhibiting a saturated candidate top-list are excluded from the sensitivities presented here.

We quote $h_{\rm sens}^{95\%}$ values rather than rigorous 95% confidence level upper limits, in order to reduce computational cost. To determine the sensitivity estimates, we use simulated signal injections to perform rigorous upper limit determination for a sampling of 0.1-Hz frequency bands (1000 injections per 0.1-Hz band) distributed over the search range; 84 bands were sampled for Cas A, 71 for Vela Jr. Each upper limit is derived from a signal amplitude $h_{\rm sens}^{95\%}$ that gives 95% detection efficiency for a loudest $2\bar{\mathcal{F}}$ value equal to $2\bar{\mathcal{F}}_{\rm thresh}(f)$ (given that all outliers above this threshold have been followed up and eliminated). The sampled upper limits are used to determine an approximate scale factor between nominal detector sensitivity and upper limit sensitivity for a given 0.1-Hz band, known as sensitivity depth $\mathcal{D}$ [59]:

$$\mathcal{D}(f) \equiv \frac{\sqrt{\bar{S}_h(f)}}{h_{\rm sens}^{95\%}}, \tag{11}$$

where $\sqrt{\bar{S}_h(f)}$ is an estimate of the effective strain amplitude spectral noise density. For non-stationary detector noise, we use an inverse-noise weighted estimate for each frequency bin j from the two interferometers:

$$\bar{S}_h(f_j) = \frac{\sum_i w_{ij} S_h(f_j)}{\sum_i w_{ij}}, \tag{12}$$

where i ranges over Fourier transforms of 30-minute segments of the H1 and L1 data, and w_{ij} is a weight equal to the average inverse power spectral density for 50 neighboring frequency bins $j' \neq j$ in the same Fourier trans-

f (Hz)	$\dot{f}$ (nHz/s)	$\ddot{f}$ (aHz/s^2)	f (Hz)	$\dot{f}$ (nHz/s)	$\ddot{f}$ (aHz/s^2)	f (Hz)	$\dot{f}$ (nHz/s)	$\ddot{f}$ (aHz/s^2)	f (Hz)	$\dot{f}$ (nHz/s)	$\ddot{f}$ (aHz/s^2)
20.0010	−0.19	−1.4	40.5022	−0.40	1.9	90.0002	−0.35	−3.0	612.1648	−3.19	2.9
21.2899	−0.10	−26.8	40.7002	−0.71	−3.2	96.0010	−1.12	0.7	614.7653	−3.77	3.7
22.2618	−0.19	−16.8	43.8618	−0.43	1.0	107.2955	−1.01	−8.8	629.8914	−18.55	6.2
22.6708	−0.53	1.2	45.0022	−0.35	−16.4	130.9282	−0.94	−18.8	651.2010	−7.28	7.6
23.6569	−0.57	−24.6	50.5949	−0.44	−5.9	299.3549	−11.33	3.0	652.8396	−1.20	−8.6
24.6429	−0.59	0.3	51.1027	−0.53	6.9	487.2795	−14.83	26.2	*861.6319	−9.66	7.7
25.9183	−0.26	2.4	52.8106	−0.83	−1.3	*488.2895	−14.54	7.3	898.8810	−15.84	0.4
27.9117	−0.25	−3.4	53.8008	−0.95	−8.9	493.2190	−7.06	2.9	899.4151	−27.55	7.2
28.9086	−0.29	1.9	54.7814	−0.25	0.8	*494.6662	−22.17	5.4	906.9044	−14.44	5.2
29.8928	−0.20	3.3	57.0029	−0.50	−8.1	499.9158	−4.49	−21.5	910.0385	−17.82	12.3
35.8866	−0.24	−21.4	60.7141	−0.51	−6.0	504.0999	−12.64	7.1	918.7510	−16.75	4.1
37.5019	−0.35	−1.5	67.0034	−0.63	−0.9	510.9000	−2.30	13.1	918.8933	−27.56	3.5
38.5020	−0.37	0.2	68.0035	−0.66	2.6	519.2834	−14.17	6.2	945.2994	−7.15	20.0
38.8775	−0.38	0.9	73.4020	−0.03	−1.7	519.2962	−10.62	5.5	945.3565	−17.64	1.7
38.9301	−0.07	−28.6	74.6306	−0.70	0.5	520.5149	−5.31	14.3			
39.8743	−0.39	1.5	85.6896	−1.06	−3.7	521.6642	−18.22	3.0			

TABLE VIII. Frequency parameters for the loudest Vela Jr. outlier in each cluster that survived round 2 follow-up. Outliers marked with asterisks were followed up with a third round.

form i:

$$w_{ij} \equiv \frac{1}{50} \sum_{j'} \frac{1}{S_h(f_{j'})} \tag{13}$$

for $|j'-j| \leq 25$ and $j' \neq j$. This weighting de-emphasizes noisy segments of data, similarly to the weighting used to define the $\mathcal{F}$-statistic. Figure 5 shows the full distributions in the resulting sensitivity depths for Cas A and Vela Jr. over the span of the search space, including significant spread from a slow decline in depth with increasing frequency due to the higher threshold $2\bar{\mathcal{F}}_{\rm thresh}(f)$. From simple linear fits to depth *vs.* frequency, we determine frequency-dependent scale factors which have values at 500 Hz of $\mathcal{D}_{\rm CasA} = 72.4$ Hz$^{-\frac{1}{2}}$ and $\mathcal{D}_{\rm VelaJr} = 81.2$ Hz$^{-\frac{1}{2}}$ with slopes of -4.8×10^{-3} Hz$^{-\frac{3}{2}}$ and -5.6×10^{-3} Hz$^{-\frac{3}{2}}$, respectively. The ratio of depths $\mathcal{D}_{\rm VelaJr}/\mathcal{D}_{\rm CasA}$ = 1.12±0.01 at 500 Hz is consistent with the approximate expected ratio of $[(7.5 \text{ days})/(5.0 \text{ days})]^{1/4} = 1.11$ for these semi-coherent searches.

VI. CONCLUSIONS

We have performed the deepest search to date for continuous gravitational waves from compact stars in the centers of the Cassiopeia A and Vela Jr. supernova remnants. Our search yieded no detections.

The achieved 95%-efficiency sensitivities are well below the age-based strain amplitude limits for these stars over virtually the entire search band of 20–976 Hz. These sensitivities are shown in Figure 6 for both sources and reach as low as $\sim 6.3 \times 10^{-26}$ for Cas A and $\sim 5.6 \times 10^{-26}$ for Vela Jr. at frequencies near 166 Hz at 95% efficiency. Conservative uncertainty bands of ±7% are indicated, to account for uncertainties in strain calibration and potential errors in frequency-dependent sensitivity depths. We have achieved the best sensitivities to date for these sources, reaching 2-3 times below the most sensitive previous results from the O1 data for Cas A. For Vela Jr. we reach ∼30% below the most sensitive previous results from the O3 data for frequencies below 600 Hz and more than 2 times below the most sensitive previous results from the O1 data for Vela Jr. up to 976 Hz.

These sensitivities are translated from strain to equatorial ellipticity ϵ using Equation 5, assuming a source distance of 3.3 kpc for Cas A, along with both 1.0 kpc and 0.2 kpc for Vela Jr., as shown in Figure 7. Under an r-modes emission assumption, the strain sensitivities can similarly be translated to r-mode amplitude α, shown in Fig. 8.

As the LIGO, Virgo and KAGRA gravitational wave detectors improve their strain sensitivities in the coming decade [62], searches will probe still smaller neutron star deformations, offering improved prospects of discovery.

VII. ACKNOWLEDGMENTS

We thank the anonymous journal referee for helpful comments, expecially concerning the treatment of the third frequency derivative which led to a refinement of the analysis. This material is based upon work supported by NSFs LIGO Laboratory which is a major facility fully funded by the National Science Foundation. The authors also gratefully acknowledge the support of the Science and Technology Facilities Council (STFC) of the United Kingdom, the Max-Planck-Society (MPS), and the State of Niedersachsen/Germany for support of the construction of Advanced LIGO and construction and operation of the GEO 600 detector. Additional support for Advanced LIGO was provided by the Australian Research Council. The authors gratefully acknowledge

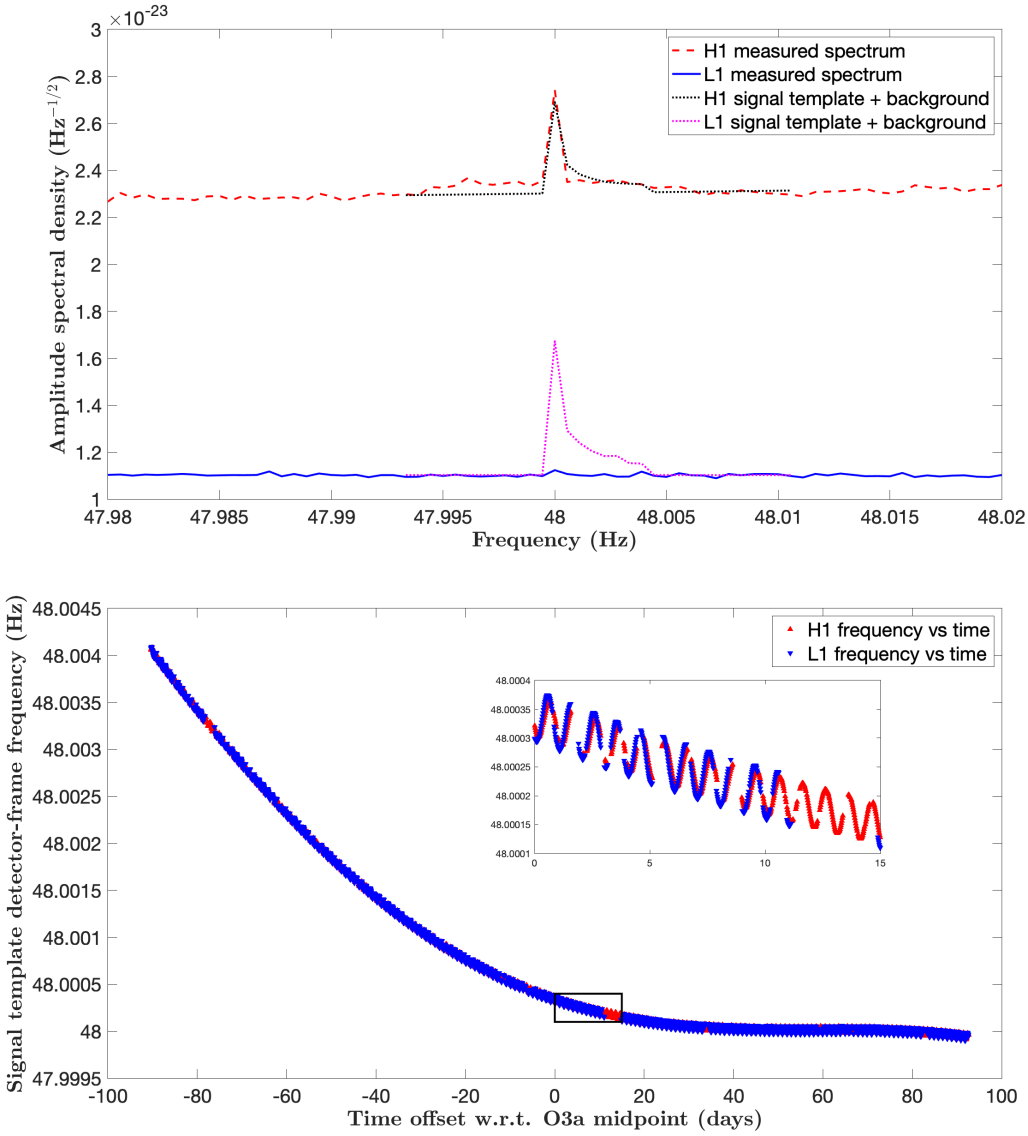

FIG. 2. Example of strain histogram and template frequency *vs.* time graphs for a Vela Jr. outlier with the same definitions (and colors) used for Cas A in Fig. 1. One key difference with respect to Cas A is that the interval of relatively stationary interferometer-frame frequency corresponding to the 48-Hz instrumental line occurs after the midpoint for Vela Jr. because of its different sky location from Cas A (color online).

the Italian Istituto Nazionale di Fisica Nucleare (INFN), the French Centre National de la Recherche Scientifique (CNRS) and the Netherlands Organization for Scientific Research (NWO), for the construction and operation of the Virgo detector and the creation and support of the EGO consortium. The authors also gratefully acknowledge research support from these agencies as well as by the Council of Scientific and Industrial Research of India, the Department of Science and Technology, India, the Science & Engineering Research Board (SERB), India, the Ministry of Human Resource Development, India, the Spanish Agencia Estatal de Investigación (AEI), the Spanish Ministerio de Ciencia e Innovación and Ministerio de Universidades, the Conselleria de Fons Europeus, Universitat i Cultura and the Direcció General de Política Universitaria i Recerca del Govern de les Illes Balears, the Conselleria d'Innovació, Universitats, Ciència i Societat Digital de la Generalitat Valenciana and the CERCA Programme Generalitat de Catalunya, Spain, the National Science Centre of Poland and the European Union European Regional Development Fund; Foundation for Polish Science (FNP), the Swiss National Science Foundation (SNSF), the Russian Foundation for Basic Research, the Russian Science Foundation, the European Commission, the European Social Funds (ESF), the European Regional Development Funds (ERDF), the Royal Society, the Scottish Funding Council, the Scottish Universities Physics Alliance, the Hungarian Scien-

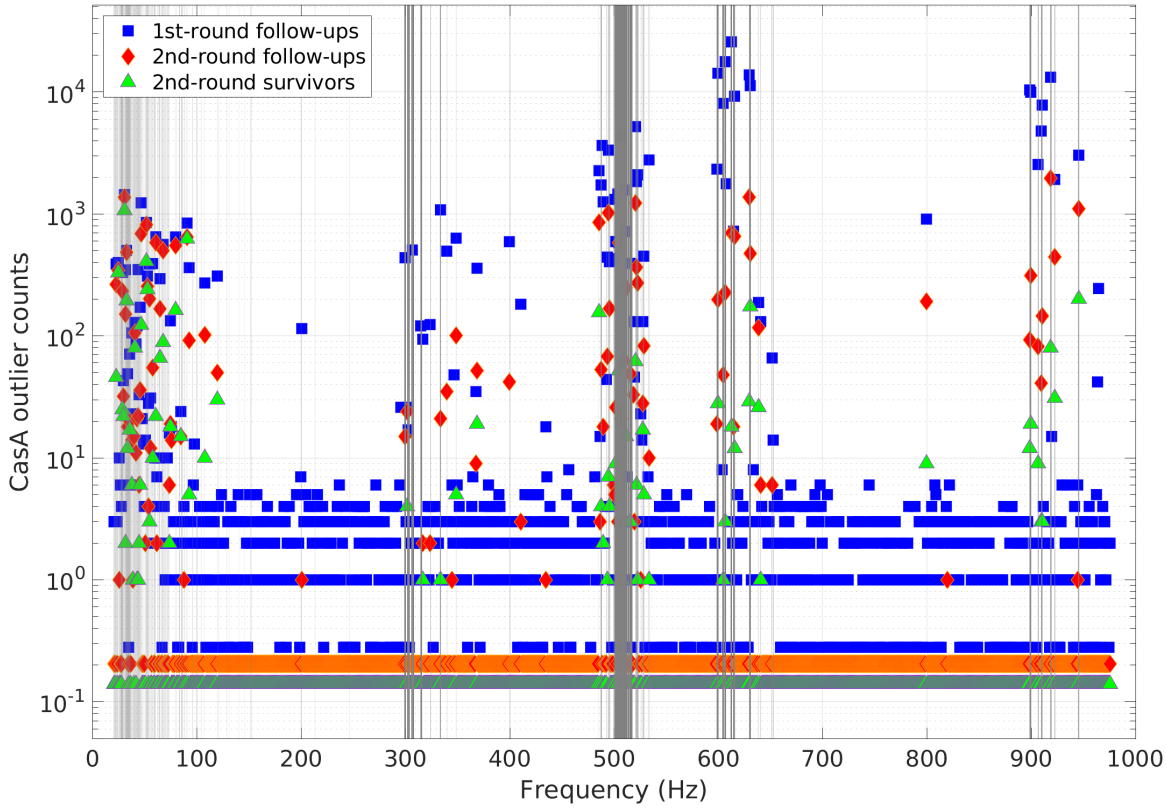

FIG. 3. Counts *vs.* frequency in 1-Hz bins for the initial Cas A search outliers (blue squares), 1st-round follow-up survivors (red diamonds) and 2nd-round follow-up survivors (green triangles). The vertical gray bands denote consolidated 0.1-Hz sub-bands displaying saturation in the initial search. One sees high outlier counts and saturations primarily at low frequencies, near test-mass violin modes (resonant vibration modes of silica fibers around 500 Hz) and at harmonics of beam-splitter violin modes (above 300 Hz and near-integer multiples). Counts equal to zero for different stages are depicted on the vertical logarithmic scale by distinct fractions less than one (color online).

tific Research Fund (OTKA), the French Lyon Institute of Origins (LIO), the Belgian Fonds de la Recherche Scientifique (FRS-FNRS), Actions de Recherche Concertes (ARC) and Fonds Wetenschappelijk Onderzoek Vlaanderen (FWO), Belgium, the Paris Île-de-France Region, the National Research, Development and Innovation Office Hungary (NKFIH), the National Research Foundation of Korea, the Natural Science and Engineering Research Council Canada, Canadian Foundation for Innovation (CFI), the Brazilian Ministry of Science, Technology, and Innovations, the International Center for Theoretical Physics South American Institute for Fundamental Research (ICTP-SAIFR), the Research Grants Council of Hong Kong, the National Natural Science Foundation of China (NSFC), the Leverhulme Trust, the Research Corporation, the Ministry of Science and Technology (MOST), Taiwan, the United States Department of Energy, and the Kavli Foundation. The authors gratefully acknowledge the support of the NSF, STFC, INFN and CNRS for provision of computational resources.

This document has been assigned LIGO Laboratory document number `LIGO-P2100298-v8`.

APPENDIX: SATURATED SUB-BANDS

As noted above, some frequency bands were so badly contaminated by instrumental lines that one or more candidate top-lists from $\dot{f}$ sub-ranges are saturated ($\geq$1000 candidates) in the initial search. All 0.1-Hz bands with saturation for the two sources searched are listed in a consolidated format in Tables IX–X and were visually examined to verify substantial instrumental contamination. We do not claim sensitivity to signals in these bands, which sum for Cas A (Vela Jr.) to 51.0 (40.9) Hz over the full search range of 20–976 Hz.

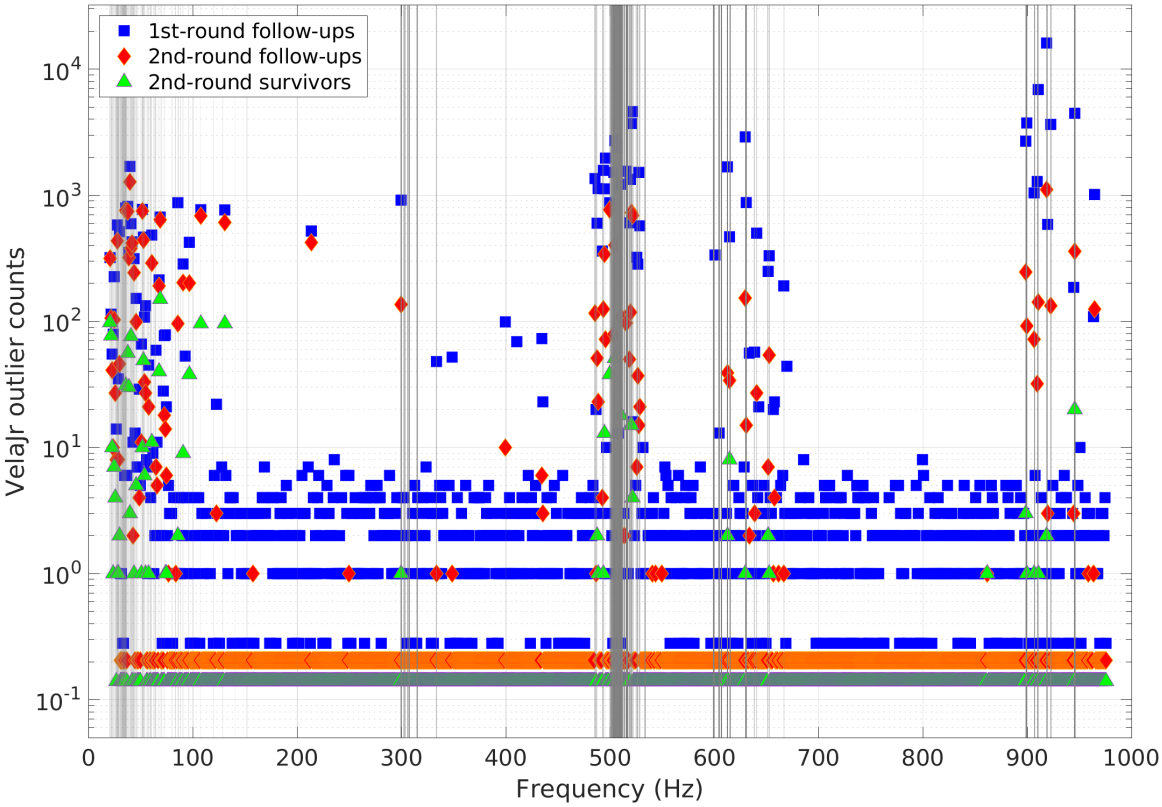

FIG. 4. Counts *vs.* frequency in 1-Hz bins for the initial Vela Jr. search outliers (blue squares), 1st-round follow-up survivors (red diamonds) and 2nd-round follow-up survivors (green triangles). The vertical gray bands denote consolidated 0.1-Hz sub-bands, as in Fig. 3 Counts equal to zero for different stages are depicted on the vertical logarithmic scale by distinct fractions less than one (color online).

$f_{\rm low}$ (Hz)	Δf (Hz)	$f_{\rm low}$ (Hz)	Δf (Hz)	$f_{\rm low}$ (Hz)	Δf (Hz)	$f_{\rm low}$ (Hz)	Δf (Hz)	$f_{\rm low}$ (Hz)	Δf (Hz)	$f_{\rm low}$ (Hz)	Δf (Hz)	$f_{\rm low}$ (Hz)	Δf (Hz)	$f_{\rm low}$ (Hz)	Δf (Hz)	$f_{\rm low}$ (Hz)	Δf (Hz)	$f_{\rm low}$ (Hz)	Δf (Hz)
20.1	0.1	28.9	0.1	36.9	0.2	45.5	0.2	56.6	0.1	70.0	0.2	119.8	0.1	339.7	0.2	515.0	2.2	638.3	0.1
20.7	0.2	29.5	0.1	37.4	0.1	46.0	0.2	56.9	0.1	70.9	0.1	121.0	0.1	348.5	0.1	520.4	0.1	640.4	0.1
21.2	0.1	29.8	0.2	38.3	0.2	46.9	0.1	57.5	0.1	71.7	0.1	128.5	0.1	399.9	0.1	520.7	0.1	651.1	0.1
21.4	0.1	30.2	0.2	38.7	0.1	47.9	0.1	57.9	0.1	72.1	0.1	130.9	0.1	485.2	0.1	521.4	0.2	652.7	0.1
21.8	0.2	30.5	0.1	38.9	0.1	48.9	0.1	58.9	0.1	72.5	0.2	140.2	0.1	487.4	0.2	522.6	0.2	898.6	0.2
22.3	0.1	31.1	0.1	39.4	0.1	49.9	0.1	59.4	0.3	73.3	0.1	145.3	0.1	487.9	0.1	525.7	0.1	898.9	0.4
22.7	0.2	31.4	0.2	39.7	0.1	50.9	0.2	59.9	0.2	79.7	0.1	151.7	0.2	492.5	0.1	526.3	0.1	906.6	0.3
23.5	0.2	31.7	0.4	39.9	0.1	51.2	0.1	62.4	0.1	80.0	0.1	199.9	0.1	493.0	0.2	527.3	0.1	909.8	0.4
23.9	0.1	32.3	0.1	40.3	0.2	51.7	0.3	62.8	0.1	83.2	0.4	213.2	0.1	494.7	0.1	527.9	0.1	918.5	0.4
24.1	0.2	32.5	0.3	40.6	0.1	52.3	0.1	63.6	0.1	85.1	0.1	246.2	0.1	495.1	0.1	528.2	0.2	922.5	0.2
24.6	0.1	32.9	0.7	40.8	0.2	52.5	0.2	63.9	0.1	85.6	0.4	299.2	0.8	495.3	0.1	528.5	0.1	945.1	0.2
25.6	0.1	33.9	1.1	41.6	0.1	52.9	0.1	64.2	0.3	87.9	0.2	301.9	0.6	495.9	0.1	533.3	0.2	945.5	0.2
25.9	0.3	35.1	0.1	41.8	0.2	53.3	0.2	65.8	0.2	89.9	0.1	303.0	0.6	499.8	0.3	598.6	1.3		
26.3	0.1	35.3	0.2	42.4	0.1	53.7	0.1	66.6	0.1	91.1	0.1	305.8	0.6	500.9	1.3	604.0	0.9		
26.6	0.1	35.6	0.2	42.8	0.3	54.2	0.1	66.8	0.2	95.8	0.2	307.1	0.7	502.4	3.8	606.1	0.9		
26.9	0.1	35.9	0.1	43.6	0.4	54.9	0.1	67.6	0.1	99.8	0.3	314.6	0.9	506.4	0.4	612.0	0.8		
27.2	0.8	36.2	0.3	44.4	0.3	55.6	0.1	68.3	0.2	104.3	0.1	323.9	0.1	506.9	5.2	614.5	1.0		
28.1	0.7	36.6	0.1	44.9	0.1	55.9	0.1	69.2	0.1	107.1	0.1	333.2	0.2	512.9	1.1	629.7	1.0		

TABLE IX. Frequency bands with saturation in the first stage of the Cas A search ($\geq$1000 outliers above threshold in a 0.1-Hz band for at least one sub-range of frequency derivatives. Each pair of numbers gives the lower limit of frequency and the width of the band affected. Consecutive 0.1-Hz bands are concatenated for compactness. These bands are excluded from the Cas A sensitivity curve shown in Fig. 6

$f_{\rm low}$ (Hz)	Δf (Hz)	$f_{\rm low}$ (Hz)	Δf (Hz)	$f_{\rm low}$ (Hz)	Δf (Hz)	$f_{\rm low}$ (Hz)	Δf (Hz)	$f_{\rm low}$ (Hz)	Δf (Hz)	$f_{\rm low}$ (Hz)	Δf (Hz)	$f_{\rm low}$ (Hz)	Δf (Hz)	$f_{\rm low}$ (Hz)	Δf (Hz)	$f_{\rm low}$ (Hz)	Δf (Hz)	$f_{\rm low}$ (Hz)	Δf (Hz)
20.1	0.1	27.3	0.6	36.0	0.1	43.6	0.2	56.6	0.1	79.7	0.1	303.1	0.4	503.5	0.4	524.6	0.1	652.8	0.1
20.5	0.1	28.0	0.1	36.3	0.4	44.0	0.1	56.9	0.1	80.0	0.1	305.9	0.5	504.0	1.3	525.2	0.1	666.6	0.1
20.7	0.1	28.2	0.6	36.8	0.1	44.5	0.2	57.5	0.1	83.2	0.3	307.2	0.5	505.5	0.4	525.8	0.1	898.7	0.2
21.4	0.2	29.0	0.1	37.0	0.1	45.5	0.1	58.0	0.1	85.7	0.3	314.8	0.5	506.5	0.3	526.3	0.2	899.1	0.4
21.8	0.2	29.5	0.1	37.4	0.1	46.0	0.2	59.0	0.1	87.9	0.2	333.3	0.2	507.2	0.5	527.1	0.1	906.8	0.2
22.3	0.1	29.9	0.2	38.3	0.2	46.5	0.1	59.4	0.3	89.9	0.1	400.0	0.1	507.9	1.8	527.8	0.1	910.0	0.3
22.5	0.1	30.2	0.2	38.7	0.1	48.0	0.1	59.9	0.2	91.1	0.1	485.2	0.1	510.0	1.9	528.3	0.2	918.7	0.3
22.7	0.1	30.5	0.1	39.7	0.1	50.0	0.1	62.4	0.1	95.8	0.2	485.7	0.1	513.2	0.6	533.3	0.2	922.6	0.2
23.5	0.1	30.9	0.1	40.0	0.1	50.9	0.2	62.8	0.1	99.9	0.2	486.4	0.1	515.2	1.0	598.9	0.8	945.2	0.2
24.0	0.1	31.2	0.1	40.3	0.2	51.6	0.3	63.6	0.1	107.1	0.1	487.2	0.2	516.5	0.5	604.2	0.5	945.6	0.2
24.2	0.1	31.4	0.2	40.6	0.1	52.0	0.1	64.0	0.1	119.8	0.1	492.6	0.1	518.4	0.1	606.4	0.5		
24.5	0.1	31.7	0.4	40.8	0.3	52.3	0.1	64.2	0.3	128.5	0.1	493.1	0.2	519.2	0.1	612.3	0.4		
25.5	0.2	32.3	0.1	41.6	0.1	52.5	0.2	66.7	0.1	140.2	0.1	493.8	0.1	519.9	0.1	614.7	0.6		
26.0	0.2	32.5	1.1	41.8	0.1	53.3	0.2	68.3	0.1	151.7	0.2	495.1	0.1	520.4	0.2	629.8	0.8		
26.3	0.1	33.8	0.5	42.0	0.1	53.7	0.1	69.4	0.1	199.9	0.2	499.9	0.2	520.7	0.1	638.3	0.1		
26.5	0.2	34.4	0.5	42.4	0.2	55.6	0.1	70.1	0.1	299.3	0.8	501.1	0.9	521.6	0.1	640.5	0.1		
26.9	0.2	35.0	0.8	42.8	0.3	56.0	0.1	72.5	0.2	302.1	0.3	502.6	0.8	522.5	0.1	651.1	0.1		

TABLE X. Frequency bands with saturation in the first stage of the Vela Jr. search ($\geq$1000 outliers above threshold in a 0.1-Hz band for at least one sub-range of frequency derivatives. Each pair of numbers gives the lower limit of frequency and the width of the band affected. Consecutive 0.1-Hz bands are concatenated for compactness. These bands are excluded from the Vela Jr. sensitivity curve shown in Fig. 6

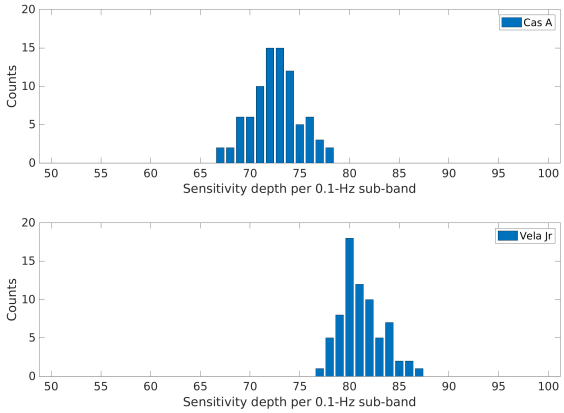

FIG. 5. Aggregated distributions of sensitivity depths (Eq. 11) for Cas A (upper) and Vela Jr. (lower) based on 84 and 71 samples, respectively, of 0.1-Hz search sub-bands spanning the full 20–976 search band. The widths of the distributions are dominated by the depth variation with respect to frequency, which we empirically fit to a linear function of negative slope.

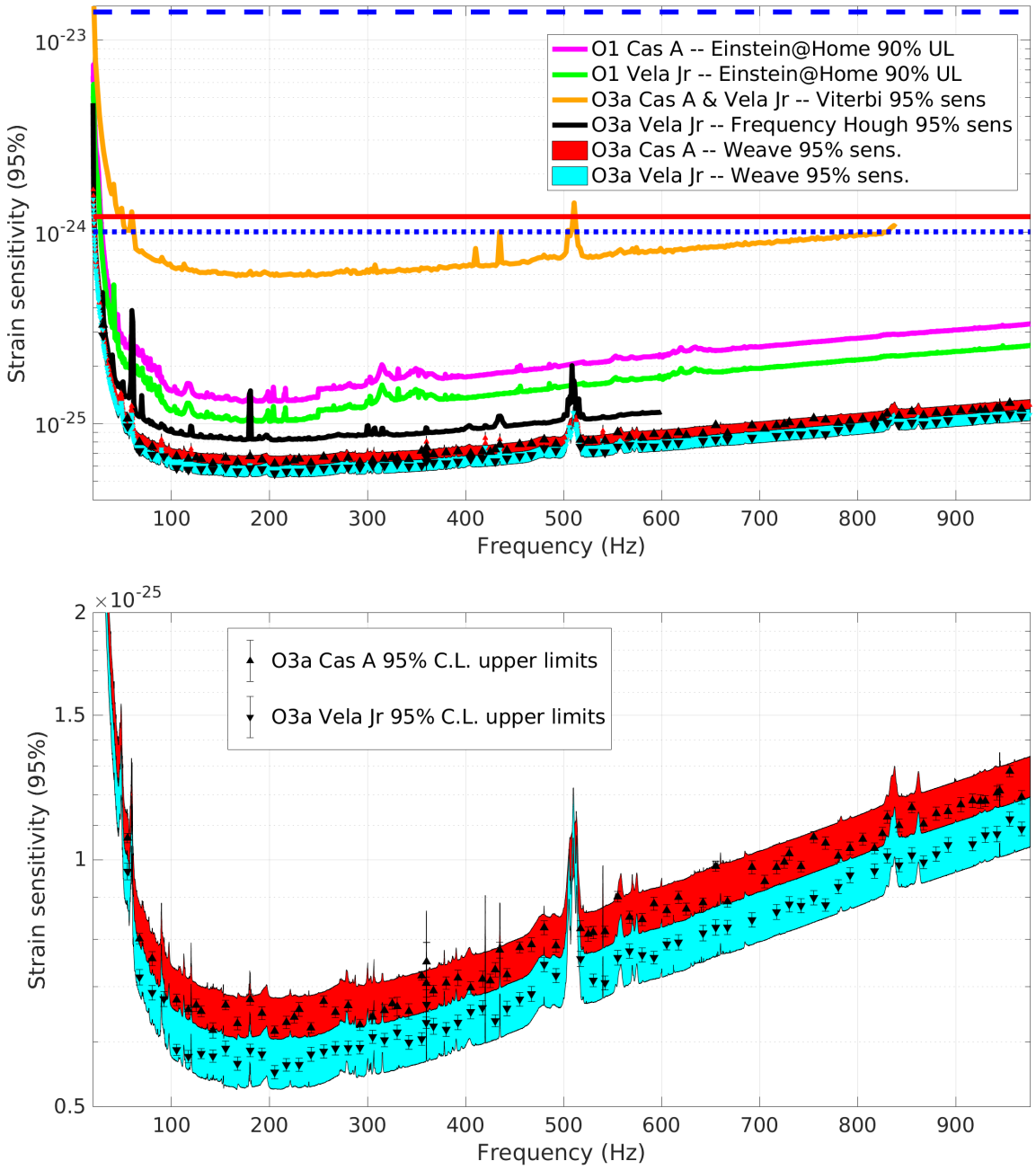

FIG. 6. *Top panel:* Estimated gravitational wave strain amplitude sensitivities (95% efficiency) in each 0.1-Hz sub-band for the Cas A (red band) and Vela Jr. (cyan band) searches. Conservative uncertainty bands of ±7% are indicated, to account for statistical and systematic uncertainties in estimating sensitivity depths, including calibration uncertainties. Black triangles (upright – Cas A, inverted – Vela Jr.) denote 0.1-Hz bands for which rigorous upper limits are used to determine estimated sensitivity *vs.* frequency. Sensitivities are estimated for only sub-bands with no saturation of the candidate top-list (see Figs. 3-4). Sensitivities are based on the absence of any outlier exceeding the frequency-dependent threshold and surviving all stages of follow-up, using the sensitivity depths (see Fig. 5) estimated in sample bands and rescaled according to the run-average amplitude spectral noise density (H1 and L1 data combined, see Eq. 12). Additional results from prior searches for Cas A and Vela Jr. are also shown: O1 Einstein@Home 90% C.L. upper limits for Cas A (magenta curve) and for Vela Jr. (green curve) [8]; O3a Cas A and Vela Jr. 95% C.L. upper limits using a model-robust Viterbi method (orange curve) [11]; O3a Vela Jr. 95% C.L. upper limits using the template-based Frequency Hough method (black curve) [11]. The solid red horizontal line indicates the age-based upper limit on Cas A strain amplitude. The dashed (dotted) horizonal blue lines indicate the optimistic (pessimistic) age-based upper limit on Vela Jr. strain amplitude, assuming an age and distance of 700 yr and 0.2 kpc (5100 yr and 1.0 kpc). *Bottom panel:* Magnification of the sensitivity bands from this analyis over most of the search band (∼40–976 Hz), with 1-σ statistical uncertainties shown for the individual sparsely sampled upper limits used to estimate the depth.

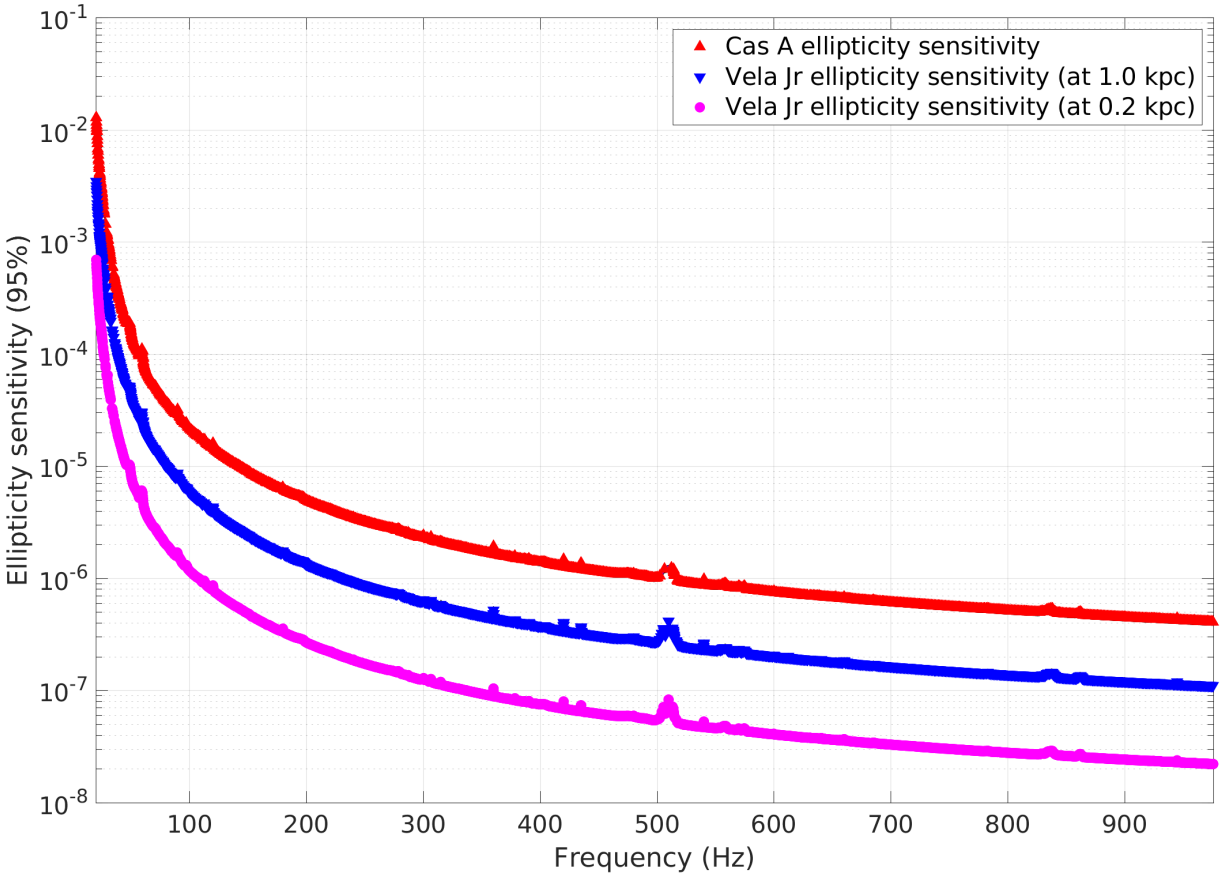

FIG. 7. Estimated equatorial ellipticity sensitivities (95% efficiency) in each 0.1-Hz sub-band for the Cas A (red) and Vela Jr. (blue, magenta) searches, derived from the strain amplitude sensitivities shown in Fig. 6 assuming a source distance of 3.3 kpc for Cas A, and assuming source distances of 1.0 kpc and 0.2 kpc for Vela Jr. (color online).

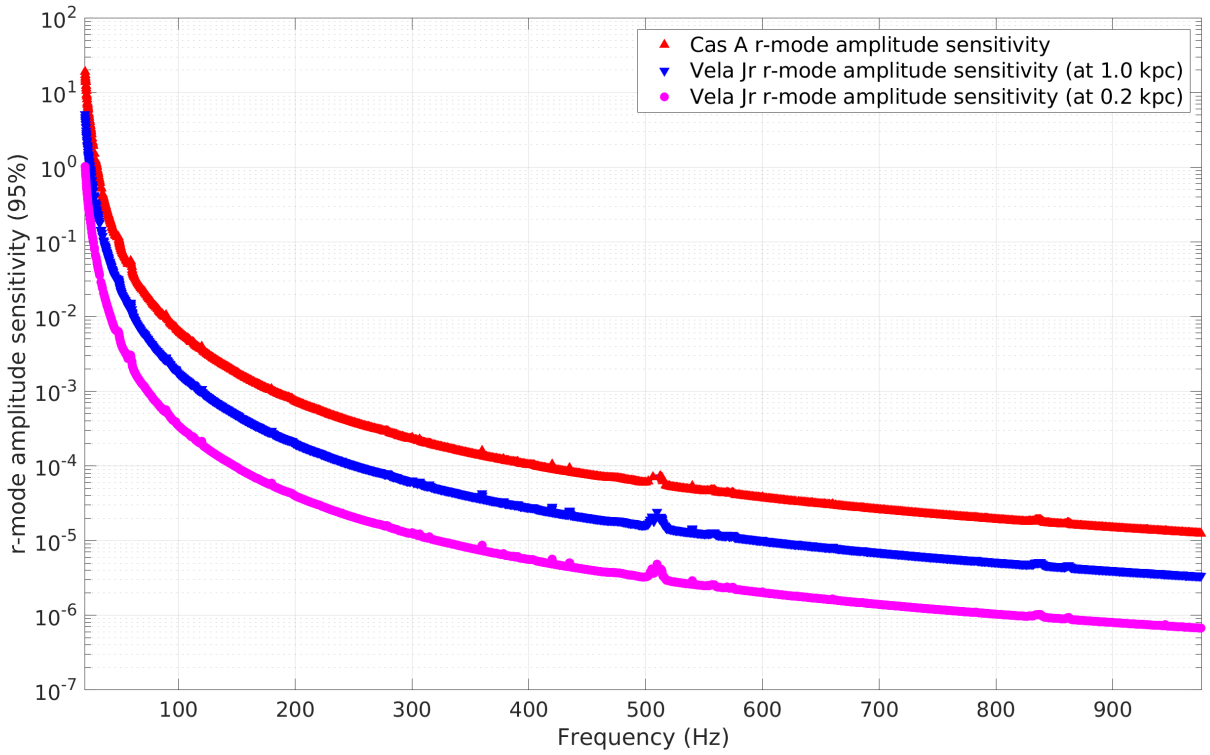

FIG. 8. Estimated r-modes amplitude α sensitivities (95% efficiency) in each 0.1-Hz sub-band for the Cas A (red) and Vela Jr. (blue, magenta) searches, derived from the strain amplitude sensitivities shown in Fig. 6 assuming a source distance of 3.3 kpc for Cas A, and assuming source distances of 1.0 kpc and 0.2 kpc for Vela Jr. (color online).

[1] M. Ryle and F.G. Smith, A New Intense Source of Radio-Frequency Radiation in the Constellation of Cassiopeia, Nat. **162**, 462 (1948).

[2] A.F. Iyudin *et al.*, Emission from ^{44}Ti associated with a previously unknown Galactic supernova, Nat. **396**, 142 (1998).

[3] D.W. Hughes, Did Flamsteed see the Cassiopeia A supernova?, Nat. **285**, 132 (1980).

[4] R.A. Fesen *et al.*, The Expansion Asymmetry and Age of the Cassiopeia A Supernova Remnant, Astroph. J, 645, 283

[5] J. Abadie *et al.*(LIGO Scientific Collaboration and Virgo Collaboration), First search for gravitational waves from the youngest known neutron star, Astroph. J. **722**, 1504 (2010).

[6] J. Aasi *et al.*(LIGO Scientific Collaboration and Virgo Collaboration), Astroph. J **813**, 39 (2015).

[7] B.P. Abbott *et al.*(LIGO Scientific Collaboration and Virgo Collaboration), Searches for Continuous Gravitational Waves from 15 Supernova Remnants and Fomalhaut b with Advanced LIGO, Astroph. J. **875**, 122 (2019).

[8] J. Ming *et al.*, Results from an Einstein@Home search for continuous gravitational waves from Cassiopeia A, Vela Jr. and G347.3, Phys. Rev. D", **100**, 024063 (2019).

[9] M.A. Papa *et al.*, Search for Continuous Gravitational Waves from the Central Compact Objects in Supernova Remnants Cassiopeia A, Vela Jr., and G347.3–0.5, Astrophys. J. **897**, 22 (2020).

[10] M. Millhouse, L. Strang and A. Melatos, Search for gravitational waves from twelve young supernova remnants with a hidden Markov model in Advanced LIGO's second observing run, Phys. Rev. D **102**, 083025 (2020).

[11] R. Abbott *et al.*, Searches for continuous gravitational waves from young supernova remnants in the early third observing run of Advanced LIGO and Virgo, Astrophys. J. **921**, 80 (2021).

[12] M. Ruderman, Neutron starquakes and pulsar periods, Nat. **223**, 597 (1969).

[13] G. Baym *et al.*, Spin up in neutron stars: The future of the vela pulsar, Nat. **224**, 872 (1969).

[14] V,R. Pandharipande, D. Pines and R.A. Smith, Neutron star structure: theory, observation, and speculation, Astroph. J. **208**, 550 (1976).

[15] M. Zimmermann, Revised estimate of gravitational radiation from Crab and Vela pulsars, Nat. **271**, 524, (1978).

[16] C. Cutler, Gravitational waves from neutron stars with large toroidal B fields, Phys. Ref. D **66**, 084025 (2002).

[17] B. Haskell *et al.*, Detecting gravitational waves from mountains on neutron stars in the Advanced Detector Era, Mon. Not. Roy. Astron. Soc. **450**, 2393 (2015).

[18] F.J. Fattoyev, C.J. Horowitz and H. Lu, Crust breaking and the limiting rotational frequency of neutron stars, arXiv:1804.04952, April 2018.

[19] N. Singh *et al.*, Asymmetric accretion and thermal mountains in magnetized neutron star crusts, Mon. Not. Roy. Astron. Soc. **493**, 3866 (2020).

[20] J. Ming *et al.*, Optimal directed searches for continuous gravitational waves, Phys. Rev. D **93**, 064011 (2016).

[21] N. Andersson, A New class of unstable modes of rotating relativistic stars, Astroph. J. **502**, 708 (1998).

[22] L. Bildsten, Gravitational radiation and rotation of accreting neutron stars, Astroph. J. Lett. **501**, L89 (1998).

[23] J.L. Friedman and S.M. Morsink, Axial instability of rotating relativistic stars, Astroph. J. **502**, 714 (1998).

[24] B.J. Owen *et al.*, Gravitational waves from hot young rapidly rotating neutron stars, Phys. Rev. D **58**, 084020 (1998).

[25] Y. Kojima, Quasitoroidal oscillations in rotating relativistic stars, Mon. Not. Roy. Astron. Soc. **293**, 49 (1998).

[26] J. Aasi *et al.* (LIGO Scientific Collaboration), Advanced LIGO, Class. Quantum Grav. **32** 7 (2015).

[27] GW150914: The Advanced LIGO Detectors in the Era of First Discoveries, B. P. Abbott *et al.* (LIGO Scientific Collaboration and Virgo Collaboration), Phys. Rev. Lett. **116**, 131103 (2016).

[28] A. Buikema *et al.*, Sensitivity and performance of the Advanced LIGO detectors in the third observing run, Phys. Rev. D **102**, 062003 (2020).

[29] M. Tse *et al.*, Quantum-Enhanced Advanced LIGO Detectors in the Era of Gravitational-Wave Astronomy, Phys. Rev. Lett. **123**, 231107 (2019).

[30] P. Lasky, Gravitational waves from neutron stars: A review, Pub. Astron. Soc. Aust. **32**, e034 (2015).

[31] K. Glampedakis and L. Gualtieri, Gravitational waves from single neutron stars: an advanced detector era survey, Astroph. Space Sci. Lib. **457** 673-736 (2018).

[32] K. Wette *et al.*, Searching for gravitational waves from Cassiopeia A with LIGO, Class. Quant. Grav. **25**, 235011 (2008).

[33] H. Tananbaum, Cassiopeia A, I.A.U. Circ. **7246**, 1 (1999).

[34] W. Ho *et al.*, X-ray bounds on cooling, composition, and magnetic field of the Cassiopeia A neutron star and young central compact objects, Mon. Not. Roy. Astron. Soc. **506**, 5015 (2021).

[35] J.P. Halpern and E.V. Gotthelf, Spin-Down Measurement of PSR J1852+0040 in Kesteven 79: Central Compact Objects as Anti-Magnetars, Astroph. J. **709**, 436 (2010).

[36] J.E. Reed *et al.*, The Three-dimensional Structure of the Cassiopeia A Supernova Remnant. I. The Spherical Shell, Astroph. J. **440**, 706 (1995).

[37] A. Alarie, A. Bilodeau and L. Drissen, A hyperspectral view of Cassiopeia A, Mon. Not. Roy. Astron. Soc. **441**, 2996 (2014).

[38] G.G Pavlov *et al.*, The compact central source in the rx j0852-4622 supernova remnant, Astrophys. J. Lett. **559**, L131 (2001).

[39] G.E. Allen *et al.*, On the Expansion Rate, Age, and Distance of the Supernova Remnant G266.2-1.2 (Vela Jr.), Astroph. J. **798**, 82 (2015).

[40] O. Kargaltsev *et al.*, The Compact Central Object in the Supernova Remnant G266.2-1.2, Astroph. J. **580**, 1060 (2002).

[41] W. Becker *et al.*, Exploring the Central Compact Object in the RX J0852.0-4622 Supernova Remnant with XMM-Newton, astro-ph/0607081, July 2006.

[42] K. Wette *et al.*, Implementing a semicoherent search for continuous gravitational waves using optimally-constructed template banks, Phys. Rev. D **97**, 123016 (2018).

[43] P. Jaranowski, A. Krolak and B.F. Schutz, Data analysis of gravitational-wave signals from spinning neutron stars. 1. The Signal and its detection, Phys. Rev. D **58**, 063001 (1998).
[44] L. Sun *et al.*, Characterization of systematic error in Advanced LIGO calibration, Class. Quant. Grav. **37**, 225008 (2020).
[45] P. Covas *et al.*, Identification and mitigation of narrow spectral artifacts that degrade searches for persistent gravitational waves in the first two observing runs of Advanced LIGO, Phys. Rev. D **97** 082002 (2018).
[46] E. Goetz *et al.*, O3a lines and combs in C00 data, `https://dcc.ligo.org/LIGO-T2000719/public`.
[47] R. Abbott *et al.*(LIGO Scientific Collaboration, Virgo Collaboration and KAGRA Collaboration), All-sky Search for Continuous Gravitational Waves from Isolated Neutron Stars in the Early O3 LIGO Data, Phys. Rev. D **104**, 082004 (2021).
[48] J. Zweizig and K. Riles, Information on self-gating of $h(t)$ used in O3a continuous-wave searches, LIGO Technical Report T2000384, September 2020, `https://dcc.ligo.org/LIGO-T2000384/public`.
[49] D. Davis *et al.*, LIGO Detector Characterization in the Second and Third Observing Runs, Class. Quant. Grav. **38**, 135014 (2021).
[50] B.P. Abbott *et al.* (LIGO Scientific Collaboration), All-sky search for periodic gravitational waves in LIGO S4 data, Phys. Rev. D **77**, 022001 (2008).
[51] B.J. Owen, How to adapt broad-band gravitational-wave searches for r-modes, Phys. Rev. D **82**, 104002 (2010)
[52] http://simbad.u-strasbg.fr/simbad Object CXOU J232327.8+584842 (J2000).
[53] http://simbad.u-strasbg.fr/simbad Object CXOU 2XMM J085201.4-461753.
[54] K. Wette and R. Prix, Flat parameter-space metric for all-sky searches for gravitational-wave pulsars, Phys. Rev. D **88**, 123005 (2013).
[55] K. Wette, Parameter-space metric for all-sky semi-coherent searches for gravitational-wave pulsars, Phys. Rev. D **92**, 082003 (2015).
[56] K. Wette, Lattice template placement for coherent all-sky searches for gravitational-wave pulsars, Phys. Rev. D **90**, 122010 (2014).
[57] D. Keitel *et al.*, Search for continuous gravitational waves: Improving robustness versus instrumental artifacts, Phys. Rev. D **89**, 064023 (2014).
[58] D. Keitel and R. Prix, Line-robust statistics for continuous gravitational waves: safety in the case of unequal detector sensitivities, Class. Quant. Grav. **32**, 035004 (2015).
[59] B. Benhke, M.A. Papa and R. Prix, Postprocessing methods used in the search for continuous gravitational-wave signals from the Galactic Center, Phys. Rev. D **91**, 064007 (2015).
[60] C. Biwer *et al.*, Validating gravitational-wave detections: The Advanced LIGO hardware injection system, Phys. Rev. D **95**, 062002 (2017).
[61] Gravitational Wave Open Science Center, `https://www.gw-openscience.org`; see also: R. Abbott *et al.*, Open data from the first and second observing runs of Advanced LIGO and Advanced Virgo, SoftwareX **13**, 100658 (2021).
[62] B.P. Abbott *et al.* (KAGRA Collaboration, LIGO Scientific Collaboration and Virgo Collaboration), Prospects for Observing and Localizing Gravitational-Wave Transients with Advanced LIGO, Advanced Virgo and KAGRA Liv. Rev. Rel. **23**, 3 (2020).

Authors

R. Abbott,[1] T. D. Abbott,[2] F. Acernese,[3,4] K. Ackley,[5] C. Adams,[6] N. Adhikari,[7] R. X. Adhikari,[1] V. B. Adya,[8] C. Affeldt,[9,10] D. Agarwal,[11] M. Agathos,[12,13] K. Agatsuma,[14] N. Aggarwal,[15] O. D. Aguiar,[16] L. Aiello,[17] A. Ain,[18] P. Ajith,[19] S. Albanesi,[20] A. Allocca,[21,4] P. A. Altin,[8] A. Amato,[22] C. Anand,[5] S. Anand,[1] A. Ananyeva,[1] S. B. Anderson,[1] W. G. Anderson,[7] T. Andrade,[23] N. Andres,[24] T. Andrić,[25] S. V. Angelova,[26] S. Ansoldi,[27,28] J. M. Antelis,[29] S. Antier,[30] S. Appert,[1] K. Arai,[1] M. C. Araya,[1] J. S. Areeda,[31] M. Arène,[30] N. Arnaud,[32,33] S. M. Aronson,[2] K. G. Arun,[34] Y. Asali,[35] G. Ashton,[5] M. Assiduo,[36,37] S. M. Aston,[6] P. Astone,[38] F. Aubin,[24] C. Austin,[2] S. Babak,[30] F. Badaracco,[39] M. K. M. Bader,[40] C. Badger,[41] S. Bae,[42] A. M. Baer,[43] S. Bagnasco,[20] Y. Bai,[1] J. Baird,[30] M. Ball,[44] G. Ballardin,[33] S. W. Ballmer,[45] A. Balsamo,[43] G. Baltus,[46] S. Banagiri,[47] D. Bankar,[11] J. C. Barayoga,[1] C. Barbieri,[48,49,50] B. C. Barish,[1] D. Barker,[51] P. Barneo,[23] F. Barone,[52,4] B. Barr,[53] L. Barsotti,[54] M. Barsuglia,[30] D. Barta,[55] J. Bartlett,[51] M. A. Barton,[53] I. Bartos,[56] R. Bassiri,[57] A. Basti,[58,18] M. Bawaj,[59,60] J. C. Bayley,[53] A. C. Baylor,[7] M. Bazzan,[61,62] B. Bécsy,[63] V. M. Bedakihale,[64] M. Bejger,[65] I. Belahcene,[32] V. Benedetto,[66] D. Beniwal,[67] T. F. Bennett,[68] J. D. Bentley,[14] M. BenYaala,[26] F. Bergamin,[9,10] B. K. Berger,[57] S. Bernuzzi,[13] D. Bersanetti,[69] A. Bertolini,[40] J. Betzwieser,[6] D. Beveridge,[70] R. Bhandare,[71] U. Bhardwaj,[72,40] D. Bhattacharjee,[73] S. Bhaumik,[56] I. A. Bilenko,[74] G. Billingsley,[1] S. Bini,[75,76] R. Birney,[77] O. Birnholtz,[78] S. Biscans,[1,54] M. Bischi,[36,37] S. Biscoveanu,[54] A. Bisht,[9,10] B. Biswas,[11] M. Bitossi,[33,18] M.-A. Bizouard,[79] J. K. Blackburn,[1] C. D. Blair,[70,6] D. G. Blair,[70] R. M. Blair,[51] F. Bobba,[80,81] N. Bode,[9,10] M. Boer,[79] G. Bogaert,[79] M. Boldrini,[82,38] L. D. Bonavena,[61] F. Bondu,[83] E. Bonilla,[57] R. Bonnand,[24] P. Booker,[9,10] B. A. Boom,[40] R. Bork,[1] V. Boschi,[18] N. Bose,[84] S. Bose,[11] V. Bossilkov,[70] V. Boudart,[46] Y. Bouffanais,[61,62] A. Bozzi,[33] C. Bradaschia,[18] P. R. Brady,[7] A. Bramley,[6] A. Branch,[6] M. Branchesi,[25,85] J. E. Brau,[44] M. Breschi,[13] T. Briant,[86] J. H. Briggs,[53] A. Brillet,[79] M. Brinkmann,[9,10] P. Brockill,[7] A. F. Brooks,[1] J. Brooks,[33] D. D. Brown,[67] S. Brunett,[1] G. Bruno,[39] R. Bruntz,[43] J. Bryant,[14] T. Bulik,[87] H. J. Bulten,[40]

A. Buonanno,[88,89] R. Buscicchio,[14] D. Buskulic,[24] C. Buy,[90] R. L. Byer,[57] L. Cadonati,[91] G. Cagnoli,[22] C. Cahillane,[51] J. Calderón Bustillo,[92,93] J. D. Callaghan,[53] T. A. Callister,[94,95] E. Calloni,[21,4] J. Cameron,[70] J. B. Camp,[96] M. Canepa,[97,69] S. Canevarolo,[98] M. Cannavacciuolo,[80] K. C. Cannon,[99] H. Cao,[67] E. Capote,[45] G. Carapella,[80,81] F. Carbognani,[33] J. B. Carlin,[100] M. F. Carney,[15] M. Carpinelli,[101,102,33] G. Carrillo,[44] G. Carullo,[58,18] T. L. Carver,[17] J. Casanueva Diaz,[33] C. Casentini,[103,104] G. Castaldi,[105] S. Caudill,[40,98] M. Cavaglià,[73] F. Cavalier,[32] R. Cavalieri,[33] M. Ceasar,[106] G. Cella,[18] P. Cerdá-Durán,[107] E. Cesarini,[104] W. Chaibi,[79] K. Chakravarti,[11] S. Chalathadka Subrahmanya,[108] E. Champion,[109] C.-H. Chan,[110] C. Chan,[99] C. L. Chan,[93] K. Chan,[93] K. Chandra,[84] P. Chanial,[33] S. Chao,[110] P. Charlton,[111] E. A. Chase,[15] E. Chassande-Mottin,[30] C. Chatterjee,[70] Debarati Chatterjee,[11] Deep Chatterjee,[7] M. Chaturvedi,[71] S. Chaty,[30] H. Y. Chen,[54] J. Chen,[110] X. Chen,[70] Y. Chen,[112] Z. Chen,[17] H. Cheng,[56] C. K. Cheong,[93] H. Y. Cheung,[93] H. Y. Chia,[56] F. Chiadini,[113,81] G. Chiarini,[62] R. Chierici,[114] A. Chincarini,[69] M. L. Chiofalo,[58,18] A. Chiummo,[33] G. Cho,[115] H. S. Cho,[116] R. K. Choudhary,[70] S. Choudhary,[11] N. Christensen,[79] Q. Chu,[70] S. Chua,[8] K. W. Chung,[41] G. Ciani,[61,62] P. Ciecielag,[65] M. Cieślar,[65] M. Cifaldi,[103,104] A. A. Ciobanu,[67] R. Ciolfi,[117,62] F. Cipriano,[79] A. Cirone,[97,69] F. Clara,[51] E. N. Clark,[118] J. A. Clark,[1,91] L. Clarke,[119] P. Clearwater,[120] S. Clesse,[121] F. Cleva,[79] E. Coccia,[25,85] E. Codazzo,[25] P.-F. Cohadon,[86] D. E. Cohen,[32] L. Cohen,[2] M. Colleoni,[122] C. G. Collette,[123] A. Colombo,[48] M. Colpi,[48,49] C. M. Compton,[51] M. Constancio Jr.,[16] L. Conti,[62] S. J. Cooper,[14] P. Corban,[6] T. R. Corbitt,[2] I. Cordero-Carrión,[124] S. Corezzi,[60,59] K. R. Corley,[35] N. Cornish,[63] D. Corre,[32] A. Corsi,[125] S. Cortese,[33] C. A. Costa,[16] R. Cotesta,[89] M. W. Coughlin,[47] J.-P. Coulon,[79] S. T. Countryman,[35] B. Cousins,[126] P. Couvares,[1] D. M. Coward,[70] M. J. Cowart,[6] D. C. Coyne,[1] R. Coyne,[127] J. D. E. Creighton,[7] T. D. Creighton,[128] A. W. Criswell,[47] M. Croquette,[86] S. G. Crowder,[129] J. R. Cudell,[46] T. J. Cullen,[2] A. Cumming,[53] R. Cummings,[53] L. Cunningham,[53] E. Cuoco,[33,130,18] M. Curyło,[87] P. Dabadie,[22] T. Dal Canton,[32] S. Dall'Osso,[25] G. Dálya,[131] A. Dana,[57] L. M. DaneshgaranBajastani,[68] B. D'Angelo,[97,69] S. Danilishin,[132,40] S. D'Antonio,[104] K. Danzmann,[9,10] C. Darsow-Fromm,[108] A. Dasgupta,[64] L. E. H. Datrier,[53] S. Datta,[11] V. Dattilo,[33] I. Dave,[71] M. Davier,[32] G. S. Davies,[133] D. Davis,[1] M. C. Davis,[106] E. J. Daw,[134] R. Dean,[106] D. DeBra,[57] M. Deenadayalan,[11] J. Degallaix,[135] M. De Laurentis,[21,4] S. Deléglise,[86] V. Del Favero,[109] F. De Lillo,[39] N. De Lillo,[53] W. Del Pozzo,[58,18] L. M. DeMarchi,[15] F. De Matteis,[103,104] V. D'Emilio,[17] N. Demos,[54] T. Dent,[92] A. Depasse,[39] R. De Pietri,[136,137] R. De Rosa,[21,4] C. De Rossi,[33] R. DeSalvo,[105] R. De Simone,[113] S. Dhurandhar,[11] M. C. Díaz,[128] M. Diaz-Ortiz Jr.,[56] N. A. Didio,[45] T. Dietrich,[89,40] L. Di Fiore,[4] C. Di Fronzo,[14] C. Di Giorgio,[80,81] F. Di Giovanni,[107] M. Di Giovanni,[25] T. Di Girolamo,[21,4] A. Di Lieto,[58,18] B. Ding,[123] S. Di Pace,[82,38] I. Di Palma,[82,38] F. Di Renzo,[58,18] A. K. Divakarla,[56] A. Dmitriev,[14] Z. Doctor,[44] L. D'Onofrio,[21,4] F. Donovan,[54] K. L. Dooley,[17] S. Doravari,[11] I. Dorrington,[17] M. Drago,[82,38] J. C. Driggers,[51] Y. Drori,[1] J.-G. Ducoin,[32] P. Dupej,[53] O. Durante,[80,81] D. D'Urso,[101,102] P.-A. Duverne,[32] S. E. Dwyer,[51] C. Eassa,[51] P. J. Easter,[5] M. Ebersold,[138] T. Eckhardt,[108] G. Eddolls,[53] B. Edelman,[44] T. B. Edo,[1] O. Edy,[133] A. Effler,[6] J. Eichholz,[8] S. S. Eikenberry,[56] M. Eisenmann,[24] R. A. Eisenstein,[54] A. Ejlli,[17] E. Engelby,[31] L. Errico,[21,4] R. C. Essick,[139] H. Estellés,[122] D. Estevez,[140] Z. Etienne,[141] T. Etzel,[1] M. Evans,[54] T. M. Evans,[6] B. E. Ewing,[126] V. Fafone,[103,104,25] H. Fair,[45] S. Fairhurst,[17] A. M. Farah,[139] S. Farinon,[69] B. Farr,[44] W. M. Farr,[94,95] N. W. Farrow,[5] E. J. Fauchon-Jones,[17] G. Favaro,[61] M. Favata,[142] M. Fays,[46] M. Fazio,[143] J. Feicht,[1] M. M. Fejer,[57] E. Fenyvesi,[55,144] D. L. Ferguson,[145] A. Fernandez-Galiana,[54] I. Ferrante,[58,18] T. A. Ferreira,[16] F. Fidecaro,[58,18] P. Figura,[87] I. Fiori,[33] M. Fishbach,[15] R. P. Fisher,[43] R. Fittipaldi,[146,81] V. Fiumara,[147,81] R. Flaminio,[24,148] E. Floden,[47] H. Fong,[99] J. A. Font,[107,149] B. Fornal,[150] P. W. F. Forsyth,[8] A. Franke,[108] S. Frasca,[82,38] F. Frasconi,[18] C. Frederick,[151] J. P. Freed,[29] Z. Frei,[131] A. Freise,[152] R. Frey,[44] P. Fritschel,[54] V. V. Frolov,[6] G. G. Fronzé,[20] P. Fulda,[56] M. Fyffe,[6] H. A. Gabbard,[53] B. U. Gadre,[89] J. R. Gair,[89] J. Gais,[93] S. Galaudage,[5] R. Gamba,[13] D. Ganapathy,[54] A. Ganguly,[19] S. G. Gaonkar,[11] B. Garaventa,[69,97] C. García-Núñez,[77] C. García-Quirós,[122] F. Garufi,[21,4] B. Gateley,[51] S. Gaudio,[29] V. Gayathri,[56] G. Gemme,[69] A. Gennai,[18] J. George,[71] O. Gerberding,[108] L. Gergely,[153] P. Gewecke,[108] S. Ghonge,[91] Abhirup Ghosh,[89] Archisman Ghosh,[154] Shaon Ghosh,[7,142] Shrobana Ghosh,[17] B. Giacomazzo,[48,49,50] L. Giacoppo,[82,38] J. A. Giaime,[2,6] K. D. Giardina,[6] D. R. Gibson,[77] C. Gier,[26] M. Giesler,[155] P. Giri,[18,58] F. Gissi,[66] J. Glanzer,[2] A. E. Gleckl,[31] P. Godwin,[126] E. Goetz,[156] R. Goetz,[56] N. Gohlke,[9,10] B. Goncharov,[5,25] G. González,[2] A. Gopakumar,[157] M. Gosselin,[33] R. Gouaty,[24] D. W. Gould,[8] B. Grace,[8] A. Grado,[158,4] M. Granata,[135] V. Granata,[80] A. Grant,[53] S. Gras,[54] P. Grassia,[1] C. Gray,[51] R. Gray,[53] G. Greco,[59] A. C. Green,[56] R. Green,[17] A. M. Gretarsson,[29] E. M. Gretarsson,[29] D. Griffith,[1] W. Griffiths,[17] H. L. Griggs,[91] G. Grignani,[60,59] A. Grimaldi,[75,76] S. J. Grimm,[25,85] H. Grote,[17] S. Grunewald,[89] P. Gruning,[32] D. Guerra,[107] G. M. Guidi,[36,37] A. R. Guimaraes,[2] G. Guixé,[23] H. K. Gulati,[64] H.-K. Guo,[150] Y. Guo,[40] Anchal Gupta,[1] Anuradha Gupta,[159] P. Gupta,[40,98] E. K. Gustafson,[1] R. Gustafson,[160]

F. Guzman,[161] L. Haegel,[30] O. Halim,[28,162] E. D. Hall,[54] E. Z. Hamilton,[138] G. Hammond,[53] M. Haney,[138] J. Hanks,[51] C. Hanna,[126] M. D. Hannam,[17] O. Hannuksela,[98,40] H. Hansen,[51] T. J. Hansen,[29] J. Hanson,[6] T. Harder,[79] T. Hardwick,[2] K. Haris,[40,98] J. Harms,[25,85] G. M. Harry,[163] I. W. Harry,[133] D. Hartwig,[108] B. Haskell,[65] R. K. Hasskew,[6] C.-J. Haster,[54] K. Haughian,[53] F. J. Hayes,[53] J. Healy,[109] A. Heidmann,[86] A. Heidt,[9,10] M. C. Heintze,[6] J. Heinze,[9,10] J. Heinzel,[164] H. Heitmann,[79] F. Hellman,[165] P. Hello,[32] A. F. Helmling-Cornell,[44] G. Hemming,[33] M. Hendry,[53] I. S. Heng,[53] E. Hennes,[40] J. Hennig,[166] M. H. Hennig,[166] A. G. Hernandez,[68] F. Hernandez Vivanco,[5] M. Heurs,[9,10] S. Hild,[132,40] P. Hill,[26] A. S. Hines,[161] S. Hochheim,[9,10] D. Hofman,[135] J. N. Hohmann,[108] D. G. Holcomb,[106] N. A. Holland,[8] I. J. Hollows,[134] Z. J. Holmes,[67] K. Holt,[6] D. E. Holz,[139] P. Hopkins,[17] J. Hough,[53] S. Hourihane,[112] E. J. Howell,[70] C. G. Hoy,[17] D. Hoyland,[14] A. Hreibi,[9,10] Y. Hsu,[110] Y. Huang,[54] M. T. Hübner,[5] A. D. Huddart,[119] B. Hughey,[29] V. Hui,[24] S. Husa,[122] S. H. Huttner,[53] R. Huxford,[126] T. Huynh-Dinh,[6] B. Idzkowski,[87] A. Iess,[103,104] C. Ingram,[67] M. Isi,[54] K. Isleif,[108] B. R. Iyer,[19] V. JaberianHamedan,[70] T. Jacqmin,[86] S. J. Jadhav,[167] S. P. Jadhav,[11] A. L. James,[17] A. Z. Jan,[109] K. Jani,[168] J. Janquart,[98,40] K. Janssens,[169,79] N. N. Janthalur,[167] P. Jaranowski,[170] D. Jariwala,[56] R. Jaume,[122] A. C. Jenkins,[41] K. Jenner,[67] M. Jeunon,[47] W. Jia,[54] G. R. Johns,[43] A. W. Jones,[70] D. I. Jones,[171] J. D. Jones,[51] P. Jones,[14] R. Jones,[53] R. J. G. Jonker,[40] L. Ju,[70] J. Junker,[9,10] V. Juste,[140] C. V. Kalaghatgi,[17,98] V. Kalogera,[15] B. Kamai,[1] S. Kandhasamy,[11] G. Kang,[172] J. B. Kanner,[1] Y. Kao,[110] S. J. Kapadia,[19] D. P. Kapasi,[8] S. Karat,[1] C. Karathanasis,[173] S. Karki,[73] R. Kashyap,[126] M. Kasprzack,[1] W. Kastaun,[9,10] S. Katsanevas,[33] E. Katsavounidis,[54] W. Katzman,[6] T. Kaur,[70] K. Kawabe,[51] F. Kéfélian,[79] D. Keitel,[122] J. S. Key,[174] S. Khadka,[57] F. Y. Khalili,[74] S. Khan,[17] E. A. Khazanov,[175] N. Khetan,[25,85] M. Khursheed,[71] N. Kijbunchoo,[8] C. Kim,[176] J. C. Kim,[177] K. Kim,[178] W. S. Kim,[179] Y.-M. Kim,[180] C. Kimball,[15] M. Kinley-Hanlon,[53] R. Kirchhoff,[9,10] J. S. Kissel,[51] L. Kleybolte,[108] S. Klimenko,[56] A. M. Knee,[156] T. D. Knowles,[141] E. Knyazev,[54] P. Koch,[9,10] G. Koekoek,[40,132] S. Koley,[25] P. Kolitsidou,[17] M. Kolstein,[173] K. Komori,[54] V. Kondrashov,[1] A. Kontos,[181] N. Koper,[9,10] M. Korobko,[108] M. Kovalam,[70] D. B. Kozak,[1] V. Kringel,[9,10] N. V. Krishnendu,[9,10] A. Królak,[182,183] G. Kuehn,[9,10] F. Kuei,[110] P. Kuijer,[40] A. Kumar,[167] P. Kumar,[155] Rahul Kumar,[51] Rakesh Kumar,[64] K. Kuns,[54] S. Kuwahara,[99] P. Lagabbe,[24] D. Laghi,[58,18] E. Lalande,[184] T. L. Lam,[93] A. Lamberts,[79,185] M. Landry,[51] B. B. Lane,[54] R. N. Lang,[54] J. Lange,[145] B. Lantz,[57] I. La Rosa,[24] A. Lartaux-Vollard,[32] P. D. Lasky,[5] M. Laxen,[6] A. Lazzarini,[1] C. Lazzaro,[61,62] P. Leaci,[82,38] S. Leavey,[9,10] Y. K. Lecoeuche,[156] H. M. Lee,[115] H. W. Lee,[177] J. Lee,[115] K. Lee,[186] J. Lehmann,[9,10] A. Lemaître,[187] N. Leroy,[32] N. Letendre,[24] C. Levesque,[184] Y. Levin,[5] J. N. Leviton,[160] K. Leyde,[30] A. K. Y. Li,[1] B. Li,[110] J. Li,[15] T. G. F. Li,[93] X. Li,[112] F. Linde,[188,40] S. D. Linker,[68] J. N. Linley,[53] T. B. Littenberg,[189] J. Liu,[9,10] K. Liu,[110] X. Liu,[7] F. Llamas,[128] M. Llorens-Monteagudo,[107] R. K. L. Lo,[1] A. Lockwood,[190] L. T. London,[54] A. Longo,[191,192] D. Lopez,[138] M. Lopez Portilla,[98] M. Lorenzini,[103,104] V. Loriette,[193] M. Lormand,[6] G. Losurdo,[18] T. P. Lott,[91] J. D. Lough,[9,10] C. O. Lousto,[109] G. Lovelace,[31] J. F. Lucaccioni,[151] H. Lück,[9,10] D. Lumaca,[103,104] A. P. Lundgren,[133] J. E. Lynam,[43] R. Macas,[133] M. MacInnis,[54] D. M. Macleod,[17] I. A. O. MacMillan,[1] A. Macquet,[79] I. Magaña Hernandez,[7] C. Magazzù,[18] R. M. Magee,[1] R. Maggiore,[14] M. Magnozzi,[69,97] S. Mahesh,[141] E. Majorana,[82,38] C. Makarem,[1] I. Maksimovic,[193] S. Maliakal,[1] A. Malik,[71] N. Man,[79] V. Mandic,[47] V. Mangano,[82,38] J. L. Mango,[194] G. L. Mansell,[51,54] M. Manske,[7] M. Mantovani,[33] M. Mapelli,[61,62] F. Marchesoni,[195,59,196] F. Marion,[24] Z. Mark,[112] S. Márka,[35] Z. Márka,[35] C. Markakis,[12] A. S. Markosyan,[57] A. Markowitz,[1] E. Maros,[1] A. Marquina,[124] S. Marsat,[30] F. Martelli,[36,37] I. W. Martin,[53] R. M. Martin,[142] M. Martinez,[173] V. A. Martinez,[56] V. Martinez,[22] K. Martinovic,[41] D. V. Martynov,[14] E. J. Marx,[54] H. Masalehdan,[108] K. Mason,[54] E. Massera,[134] A. Masserot,[24] T. J. Massinger,[54] M. Masso-Reid,[53] S. Mastrogiovanni,[30] A. Matas,[89] M. Mateu-Lucena,[122] F. Matichard,[1,54] M. Matiushechkina,[9,10] N. Mavalvala,[54] J. J. McCann,[70] R. McCarthy,[51] D. E. McClelland,[8] P. K. McClincy,[126] S. McCormick,[6] L. McCuller,[54] G. I. McGhee,[53] S. C. McGuire,[197] C. McIsaac,[133] J. McIver,[156] T. McRae,[8] S. T. McWilliams,[141] D. Meacher,[7] M. Mehmet,[9,10] A. K. Mehta,[89] Q. Meijer,[98] A. Melatos,[100] D. A. Melchor,[31] G. Mendell,[51] A. Menendez-Vazquez,[173] C. S. Menoni,[143] R. A. Mercer,[7] L. Mereni,[135] K. Merfeld,[44] E. L. Merilh,[6] J. D. Merritt,[44] M. Merzougui,[79] S. Meshkov,[1,a] C. Messenger,[53] C. Messick,[145] P. M. Meyers,[100] F. Meylahn,[9,10] A. Mhaske,[11] A. Miani,[75,76] H. Miao,[14] I. Michaloliakos,[56] C. Michel,[135] H. Middleton,[100] L. Milano,[21] A. Miller,[68] A. L. Miller,[39] B. Miller,[72,40] M. Millhouse,[100] J. C. Mills,[17] E. Milotti,[162,28] O. Minazzoli,[79,198] Y. Minenkov,[104] Ll. M. Mir,[173] M. Miravet-Tenés,[107] C. Mishra,[199] T. Mishra,[56] T. Mistry,[134] S. Mitra,[11] V. P. Mitrofanov,[74] G. Mitselmakher,[56] R. Mittleman,[54] Geoffrey Mo,[54] E. Moguel,[151] K. Mogushi,[73] S. R. P. Mohapatra,[54] S. R. Mohite,[7] I. Molina,[31] M. Molina-Ruiz,[165] M. Mondin,[68] M. Montani,[36,37] C. J. Moore,[14] D. Moraru,[51] F. Morawski,[65] A. More,[11] C. Moreno,[29] G. Moreno,[51] S. Morisaki,[7] B. Mours,[140] C. M. Mow-Lowry,[14,152] S. Mozzon,[133] F. Muciaccia,[82,38] Arunava Mukherjee,[200] D. Mukherjee,[126] Soma Mukherjee,[128] Subroto Mukherjee,[64] Suvodip Mukherjee,[72]

N. Mukund,[9,10] A. Mullavey,[6] J. Munch,[67] E. A. Muñiz,[45] P. G. Murray,[53] R. Musenich,[69,97] S. Muusse,[67] S. L. Nadji,[9,10] A. Nagar,[20,201] V. Napolano,[33] I. Nardecchia,[103,104] L. Naticchioni,[38] B. Nayak,[68] R. K. Nayak,[202] B. F. Neil,[70] J. Neilson,[66,81] G. Nelemans,[203] T. J. N. Nelson,[6] M. Nery,[9,10] P. Neubauer,[151] A. Neunzert,[174] K. Y. Ng,[54] S. W. S. Ng,[67] C. Nguyen,[30] P. Nguyen,[44] T. Nguyen,[54] S. A. Nichols,[2] S. Nissanke,[72,40] E. Nitoglia,[114] F. Nocera,[33] M. Norman,[17] C. North,[17] L. K. Nuttall,[133] J. Oberling,[51] B. D. O'Brien,[56] J. O'Dell,[119] E. Oelker,[53] G. Oganesyan,[25,85] J. J. Oh,[179] S. H. Oh,[179] F. Ohme,[9,10] H. Ohta,[99] M. A. Okada,[16] C. Olivetto,[33] R. Oram,[6] B. O'Reilly,[6] R. G. Ormiston,[47] N. D. Ormsby,[43] L. F. Ortega,[56] R. O'Shaughnessy,[109] E. O'Shea,[155] S. Ossokine,[89] C. Osthelder,[1] D. J. Ottaway,[67] H. Overmier,[6] A. E. Pace,[126] G. Pagano,[58,18] M. A. Page,[70] G. Pagliaroli,[25,85] A. Pai,[84] S. A. Pai,[71] J. R. Palamos,[44] O. Palashov,[175] C. Palomba,[38] H. Pan,[110] P. K. Panda,[167] P. T. H. Pang,[40,98] C. Pankow,[15] F. Pannarale,[82,38] B. C. Pant,[71] F. H. Panther,[70] F. Paoletti,[18] A. Paoli,[33] A. Paolone,[38,204] H. Park,[7] W. Parker,[6,197] D. Pascucci,[40] A. Pasqualetti,[33] R. Passaquieti,[58,18] D. Passuello,[18] M. Patel,[43] M. Pathak,[67] B. Patricelli,[33,18] A. S. Patron,[2] S. Paul,[44] E. Payne,[5] M. Pedraza,[1] M. Pegoraro,[62] A. Pele,[6] S. Penn,[205] A. Perego,[75,76] A. Pereira,[22] T. Pereira,[206] C. J. Perez,[51] C. Périgois,[24] C. C. Perkins,[56] A. Perreca,[75,76] S. Perriès,[114] J. Petermann,[108] D. Petterson,[1] H. P. Pfeiffer,[89] K. A. Pham,[47] K. S. Phukon,[40,188] O. J. Piccinni,[38] M. Pichot,[79] M. Piendibene,[58,18] F. Piergiovanni,[36,37] L. Pierini,[82,38] V. Pierro,[66,81] G. Pillant,[33] M. Pillas,[32] F. Pilo,[18] L. Pinard,[135] I. M. Pinto,[66,81,207] M. Pinto,[33] K. Piotrzkowski,[39] M. Pirello,[51] M. D. Pitkin,[208] E. Placidi,[82,38] L. Planas,[122] W. Plastino,[191,192] C. Pluchar,[118] R. Poggiani,[58,18] E. Polini,[24] D. Y. T. Pong,[93] S. Ponrathnam,[11] P. Popolizio,[33] E. K. Porter,[30] R. Poulton,[33] J. Powell,[120] M. Pracchia,[24] T. Pradier,[140] A. K. Prajapati,[64] K. Prasai,[57] R. Prasanna,[167] G. Pratten,[14] M. Principe,[66,207,81] G. A. Prodi,[209,76] L. Prokhorov,[14] P. Prosposito,[103,104] L. Prudenzi,[89] A. Puecher,[40,98] M. Punturo,[59] F. Puosi,[18,58] P. Puppo,[38] M. Pürrer,[89] H. Qi,[17] V. Quetschke,[128] R. Quitzow-James,[73] F. J. Raab,[51] G. Raaijmakers,[72,40] H. Radkins,[51] N. Radulesco,[79] P. Raffai,[131] S. X. Rail,[184] S. Raja,[71] C. Rajan,[71] K. E. Ramirez,[6] T. D. Ramirez,[31] A. Ramos-Buades,[89] J. Rana,[126] P. Rapagnani,[82,38] U. D. Rapol,[210] A. Ray,[7] V. Raymond,[17] N. Raza,[156] M. Razzano,[58,18] J. Read,[31] L. A. Rees,[163] T. Regimbau,[24] L. Rei,[69] S. Reid,[26] S. W. Reid,[43] D. H. Reitze,[1,56] P. Relton,[17] A. Renzini,[1] P. Rettegno,[211,20] M. Rezac,[31] F. Ricci,[82,38] D. Richards,[119] J. W. Richardson,[1] L. Richardson,[161] G. Riemenschneider,[211,20] K. Riles,[160] S. Rinaldi,[18,58] K. Rink,[156] M. Rizzo,[15] N. A. Robertson,[1,53] R. Robie,[1] F. Robinet,[32] A. Rocchi,[104] S. Rodriguez,[31] L. Rolland,[24] J. G. Rollins,[1] M. Romanelli,[83] R. Romano,[3,4] C. L. Romel,[51] A. Romero-Rodríguez,[173] I. M. Romero-Shaw,[5] J. H. Romie,[6] S. Ronchini,[25,85] L. Rosa,[4,21] C. A. Rose,[7] D. Rosińska,[87] M. P. Ross,[190] S. Rowan,[53] S. J. Rowlinson,[14] S. Roy,[98] Santosh Roy,[11] Soumen Roy,[212] D. Rozza,[101,102] P. Ruggi,[33] K. Ryan,[51] S. Sachdev,[126] T. Sadecki,[51] J. Sadiq,[92] M. Sakellariadou,[41] O. S. Salafia,[50,49,48] L. Salconi,[33] M. Saleem,[47] F. Salemi,[75,76] A. Samajdar,[40,98] E. J. Sanchez,[1] J. H. Sanchez,[31] L. E. Sanchez,[1] N. Sanchis-Gual,[213] J. R. Sanders,[214] A. Sanuy,[23] T. R. Saravanan,[11] N. Sarin,[5] B. Sassolas,[135] H. Satari,[70] B. S. Sathyaprakash,[126,17] O. Sauter,[56] R. L. Savage,[51] D. Sawant,[84] H. L. Sawant,[11] S. Sayah,[135] D. Schaetzl,[1] M. Scheel,[112] J. Scheuer,[15] M. Schiworski,[67] P. Schmidt,[14] S. Schmidt,[98] R. Schnabel,[108] M. Schneewind,[9,10] R. M. S. Schofield,[44] A. Schönbeck,[108] B. W. Schulte,[9,10] B. F. Schutz,[17,9,10] E. Schwartz,[17] J. Scott,[53] S. M. Scott,[8] M. Seglar-Arroyo,[24] D. Sellers,[6] A. S. Sengupta,[212] D. Sentenac,[33] E. G. Seo,[93] V. Sequino,[21,4] A. Sergeev,[175] Y. Setyawati,[98] T. Shaffer,[51] M. S. Shahriar,[15] B. Shams,[150] A. Sharma,[25,85] P. Sharma,[71] P. Shawhan,[88] N. S. Shcheblanov,[187] M. Shikauchi,[99] D. H. Shoemaker,[54] D. M. Shoemaker,[145] S. ShyamSundar,[71] M. Sieniawska,[87] D. Sigg,[51] L. P. Singer,[96] D. Singh,[126] N. Singh,[87] A. Singha,[132,40] A. M. Sintes,[122] V. Sipala,[101,102] V. Skliris,[17] B. J. J. Slagmolen,[8] T. J. Slaven-Blair,[70] J. Smetana,[14] J. R. Smith,[31] R. J. E. Smith,[5] J. Soldateschi,[215,216,37] S. N. Somala,[217] E. J. Son,[179] K. Soni,[11] S. Soni,[2] V. Sordini,[114] F. Sorrentino,[69] N. Sorrentino,[58,18] R. Soulard,[79] T. Souradeep,[210,11] E. Sowell,[125] V. Spagnuolo,[132,40] A. P. Spencer,[53] M. Spera,[61,62] R. Srinivasan,[79] A. K. Srivastava,[64] V. Srivastava,[45] K. Staats,[15] C. Stachie,[79] D. A. Steer,[30] J. Steinlechner,[132,40] S. Steinlechner,[132,40] D. J. Stops,[14] M. Stover,[151] K. A. Strain,[53] L. C. Strang,[100] G. Stratta,[218,37] A. Strunk,[51] R. Sturani,[206] A. L. Stuver,[106] S. Sudhagar,[11] V. Sudhir,[54] H. G. Suh,[7] T. Z. Summerscales,[219] H. Sun,[70] L. Sun,[8] S. Sunil,[64] A. Sur,[65] J. Suresh,[99] P. J. Sutton,[17] B. L. Swinkels,[40] M. J. Szczepańczyk,[56] P. Szewczyk,[87] M. Tacca,[40] S. C. Tait,[53] C. J. Talbot,[26] C. Talbot,[1] A. J. Tanasijczuk,[39] D. B. Tanner,[56] D. Tao,[1] L. Tao,[56] E. N. Tapia San Martín,[40] C. Taranto,[103] J. D. Tasson,[164] R. Tenorio,[122] J. E. Terhune,[106] L. Terkowski,[108] M. P. Thirugnanasambandam,[11] M. Thomas,[6] P. Thomas,[51] J. E. Thompson,[17] S. R. Thondapu,[71] K. A. Thorne,[6] E. Thrane,[5] Shubhanshu Tiwari,[138] Srishti Tiwari,[11] V. Tiwari,[17] A. M. Toivonen,[47] K. Toland,[53] A. E. Tolley,[133] M. Tonelli,[58,18] A. Torres-Forné,[107] C. I. Torrie,[1] I. Tosta e Melo,[101,102] D. Töyrä,[8] A. Trapananti,[195,59] F. Travasso,[59,195] G. Traylor,[6] M. Trevor,[88] M. C. Tringali,[33] A. Tripathee,[160] L. Troiano,[220,81] A. Trovato,[30] L. Trozzo,[4] R. J. Trudeau,[1] D. S. Tsai,[110] D. Tsai,[110]

K. W. Tsang,[40,221,98] M. Tse,[54] R. Tso,[112] L. Tsukada,[99] D. Tsuna,[99] T. Tsutsui,[99] K. Turbang,[222,169] M. Turconi,[79] A. S. Ubhi,[14] R. P. Udall,[1] K. Ueno,[99] C. S. Unnikrishnan,[157] A. L. Urban,[2] A. Utina,[132,40] H. Vahlbruch,[9,10] G. Vajente,[1] A. Vajpeyi,[5] G. Valdes,[161] M. Valentini,[75,76] V. Valsan,[7] N. van Bakel,[40] M. van Beuzekom,[40] J. F. J. van den Brand,[132,223,40] C. Van Den Broeck,[98,40] D. C. Vander-Hyde,[45] L. van der Schaaf,[40] J. V. van Heijningen,[39] J. Vanosky,[1] N. van Remortel,[169] M. Vardaro,[188,40] A. F. Vargas,[100] V. Varma,[155] M. Vasúth,[55] A. Vecchio,[14] G. Vedovato,[62] J. Veitch,[53] P. J. Veitch,[67] J. Venneberg,[9,10] G. Venugopalan,[1] D. Verkindt,[24] P. Verma,[183] Y. Verma,[71] D. Veske,[35] F. Vetrano,[36] A. Viceré,[36,37] S. Vidyant,[45] A. D. Viets,[194] A. Vijaykumar,[19] V. Villa-Ortega,[92] J.-Y. Vinet,[79] A. Virtuoso,[162,28] S. Vitale,[54] T. Vo,[45] H. Vocca,[60,59] E. R. G. von Reis,[51] J. S. A. von Wrangel,[9,10] C. Vorvick,[51] S. P. Vyatchanin,[74] L. E. Wade,[151] M. Wade,[151] K. J. Wagner,[109] R. C. Walet,[40] M. Walker,[43] G. S. Wallace,[26] L. Wallace,[1] S. Walsh,[7] J. Z. Wang,[160] W. H. Wang,[128] R. L. Ward,[8] J. Warner,[51] M. Was,[24] N. Y. Washington,[1] J. Watchi,[123] B. Weaver,[51] S. A. Webster,[53] M. Weinert,[9,10] A. J. Weinstein,[1] R. Weiss,[54] G. Weldon,[160] C. M. Weller,[190] F. Wellmann,[9,10] L. Wen,[70] P. Weßels,[9,10] K. Wette,[8] J. T. Whelan,[109] D. D. White,[31] B. F. Whiting,[56] C. Whittle,[54] D. Wilken,[9,10] D. Williams,[53] M. J. Williams,[53] A. R. Williamson,[133] J. L. Willis,[1] B. Willke,[9,10] D. J. Wilson,[118] W. Winkler,[9,10] C. C. Wipf,[1] T. Wlodarczyk,[89] G. Woan,[53] J. Woehler,[9,10] J. K. Wofford,[109] I. C. F. Wong,[93] D. S. Wu,[9,10] D. M. Wysocki,[7] L. Xiao,[1] H. Yamamoto,[1] F. W. Yang,[150] L. Yang,[143] Yang Yang,[56] Z. Yang,[47] M. J. Yap,[8] D. W. Yeeles,[17] A. B. Yelikar,[109] M. Ying,[110] J. Yoo,[155] Hang Yu,[112] Haocun Yu,[54] A. Zadrożny,[183] M. Zanolin,[29] T. Zelenova,[33] J.-P. Zendri,[62] M. Zevin,[139] J. Zhang,[70] L. Zhang,[1] T. Zhang,[14] Y. Zhang,[161] C. Zhao,[70] G. Zhao,[123] Yue Zhao,[150] R. Zhou,[165] Z. Zhou,[15] X. J. Zhu,[5] A. B. Zimmerman,[145] M. E. Zucker,[1,54] and J. Zweizig[1]

[1] *LIGO Laboratory, California Institute of Technology, Pasadena, CA 91125, USA*
[2] *Louisiana State University, Baton Rouge, LA 70803, USA*
[3] *Dipartimento di Farmacia, Università di Salerno, I-84084 Fisciano, Salerno, Italy*
[4] *INFN, Sezione di Napoli, Complesso Universitario di Monte S. Angelo, I-80126 Napoli, Italy*
[5] *OzGrav, School of Physics & Astronomy, Monash University, Clayton 3800, Victoria, Australia*
[6] *LIGO Livingston Observatory, Livingston, LA 70754, USA*
[7] *University of Wisconsin-Milwaukee, Milwaukee, WI 53201, USA*
[8] *OzGrav, Australian National University, Canberra, Australian Capital Territory 0200, Australia*
[9] *Max Planck Institute for Gravitational Physics (Albert Einstein Institute), D-30167 Hannover, Germany*
[10] *Leibniz Universität Hannover, D-30167 Hannover, Germany*
[11] *Inter-University Centre for Astronomy and Astrophysics, Pune 411007, India*
[12] *University of Cambridge, Cambridge CB2 1TN, United Kingdom*
[13] *Theoretisch-Physikalisches Institut, Friedrich-Schiller-Universität Jena, D-07743 Jena, Germany*
[14] *University of Birmingham, Birmingham B15 2TT, United Kingdom*
[15] *Center for Interdisciplinary Exploration & Research in Astrophysics (CIERA), Northwestern University, Evanston, IL 60208, USA*
[16] *Instituto Nacional de Pesquisas Espaciais, 12227-010 São José dos Campos, São Paulo, Brazil*
[17] *Gravity Exploration Institute, Cardiff University, Cardiff CF24 3AA, United Kingdom*
[18] *INFN, Sezione di Pisa, I-56127 Pisa, Italy*
[19] *International Centre for Theoretical Sciences, Tata Institute of Fundamental Research, Bengaluru 560089, India*
[20] *INFN Sezione di Torino, I-10125 Torino, Italy*
[21] *Università di Napoli "Federico II", Complesso Universitario di Monte S. Angelo, I-80126 Napoli, Italy*
[22] *Université de Lyon, Université Claude Bernard Lyon 1, CNRS, Institut Lumière Matière, F-69622 Villeurbanne, France*
[23] *Institut de Ciències del Cosmos (ICCUB), Universitat de Barcelona, C/ Martí i Franquès 1, Barcelona, 08028, Spain*
[24] *Laboratoire d'Annecy de Physique des Particules (LAPP), Univ. Grenoble Alpes, Université Savoie Mont Blanc, CNRS/IN2P3, F-74941 Annecy, France*
[25] *Gran Sasso Science Institute (GSSI), I-67100 L'Aquila, Italy*
[26] *SUPA, University of Strathclyde, Glasgow G1 1XQ, United Kingdom*
[27] *Dipartimento di Scienze Matematiche, Informatiche e Fisiche, Università di Udine, I-33100 Udine, Italy*
[28] *INFN, Sezione di Trieste, I-34127 Trieste, Italy*
[29] *Embry-Riddle Aeronautical University, Prescott, AZ 86301, USA*
[30] *Université de Paris, CNRS, Astroparticule et Cosmologie, F-75006 Paris, France*
[31] *California State University Fullerton, Fullerton, CA 92831, USA*
[32] *Université Paris-Saclay, CNRS/IN2P3, IJCLab, 91405 Orsay, France*
[33] *European Gravitational Observatory (EGO), I-56021 Cascina, Pisa, Italy*
[34] *Chennai Mathematical Institute, Chennai 603103, India*
[35] *Columbia University, New York, NY 10027, USA*
[36] *Università degli Studi di Urbino "Carlo Bo", I-61029 Urbino, Italy*
[37] *INFN, Sezione di Firenze, I-50019 Sesto Fiorentino, Firenze, Italy*

[38] *INFN, Sezione di Roma, I-00185 Roma, Italy*
[39] *Université catholique de Louvain, B-1348 Louvain-la-Neuve, Belgium*
[40] *Nikhef, Science Park 105, 1098 XG Amsterdam, Netherlands*
[41] *King's College London, University of London, London WC2R 2LS, United Kingdom*
[42] *Korea Institute of Science and Technology Information, Daejeon 34141, Republic of Korea*
[43] *Christopher Newport University, Newport News, VA 23606, USA*
[44] *University of Oregon, Eugene, OR 97403, USA*
[45] *Syracuse University, Syracuse, NY 13244, USA*
[46] *Université de Liège, B-4000 Liège, Belgium*
[47] *University of Minnesota, Minneapolis, MN 55455, USA*
[48] *Università degli Studi di Milano-Bicocca, I-20126 Milano, Italy*
[49] *INFN, Sezione di Milano-Bicocca, I-20126 Milano, Italy*
[50] *INAF, Osservatorio Astronomico di Brera sede di Merate, I-23807 Merate, Lecco, Italy*
[51] *LIGO Hanford Observatory, Richland, WA 99352, USA*
[52] *Dipartimento di Medicina, Chirurgia e Odontoiatria "Scuola Medica Salernitana", Università di Salerno, I-84081 Baronissi, Salerno, Italy*
[53] *SUPA, University of Glasgow, Glasgow G12 8QQ, United Kingdom*
[54] *LIGO Laboratory, Massachusetts Institute of Technology, Cambridge, MA 02139, USA*
[55] *Wigner RCP, RMKI, H-1121 Budapest, Konkoly Thege Miklós út 29-33, Hungary*
[56] *University of Florida, Gainesville, FL 32611, USA*
[57] *Stanford University, Stanford, CA 94305, USA*
[58] *Università di Pisa, I-56127 Pisa, Italy*
[59] *INFN, Sezione di Perugia, I-06123 Perugia, Italy*
[60] *Università di Perugia, I-06123 Perugia, Italy*
[61] *Università di Padova, Dipartimento di Fisica e Astronomia, I-35131 Padova, Italy*
[62] *INFN, Sezione di Padova, I-35131 Padova, Italy*
[63] *Montana State University, Bozeman, MT 59717, USA*
[64] *Institute for Plasma Research, Bhat, Gandhinagar 382428, India*
[65] *Nicolaus Copernicus Astronomical Center, Polish Academy of Sciences, 00-716, Warsaw, Poland*
[66] *Dipartimento di Ingegneria, Università del Sannio, I-82100 Benevento, Italy*
[67] *OzGrav, University of Adelaide, Adelaide, South Australia 5005, Australia*
[68] *California State University, Los Angeles, 5151 State University Dr, Los Angeles, CA 90032, USA*
[69] *INFN, Sezione di Genova, I-16146 Genova, Italy*
[70] *OzGrav, University of Western Australia, Crawley, Western Australia 6009, Australia*
[71] *RRCAT, Indore, Madhya Pradesh 452013, India*
[72] *GRAPPA, Anton Pannekoek Institute for Astronomy and Institute for High-Energy Physics, University of Amsterdam, Science Park 904, 1098 XH Amsterdam, Netherlands*
[73] *Missouri University of Science and Technology, Rolla, MO 65409, USA*
[74] *Faculty of Physics, Lomonosov Moscow State University, Moscow 119991, Russia*
[75] *Università di Trento, Dipartimento di Fisica, I-38123 Povo, Trento, Italy*
[76] *INFN, Trento Institute for Fundamental Physics and Applications, I-38123 Povo, Trento, Italy*
[77] *SUPA, University of the West of Scotland, Paisley PA1 2BE, United Kingdom*
[78] *Bar-Ilan University, Ramat Gan, 5290002, Israel*
[79] *Artemis, Université Côte d'Azur, Observatoire de la Côte d'Azur, CNRS, F-06304 Nice, France*
[80] *Dipartimento di Fisica "E.R. Caianiello", Università di Salerno, I-84084 Fisciano, Salerno, Italy*
[81] *INFN, Sezione di Napoli, Gruppo Collegato di Salerno, Complesso Universitario di Monte S. Angelo, I-80126 Napoli, Italy*
[82] *Università di Roma "La Sapienza", I-00185 Roma, Italy*
[83] *Univ Rennes, CNRS, Institut FOTON - UMR6082, F-3500 Rennes, France*
[84] *Indian Institute of Technology Bombay, Powai, Mumbai 400 076, India*
[85] *INFN, Laboratori Nazionali del Gran Sasso, I-67100 Assergi, Italy*
[86] *Laboratoire Kastler Brossel, Sorbonne Université, CNRS, ENS-Université PSL, Collège de France, F-75005 Paris, France*
[87] *Astronomical Observatory Warsaw University, 00-478 Warsaw, Poland*
[88] *University of Maryland, College Park, MD 20742, USA*
[89] *Max Planck Institute for Gravitational Physics (Albert Einstein Institute), D-14476 Potsdam, Germany*
[90] *L2IT, Laboratoire des 2 Infinis - Toulouse, Université de Toulouse, CNRS/IN2P3, UPS, F-31062 Toulouse Cedex 9, France*
[91] *School of Physics, Georgia Institute of Technology, Atlanta, GA 30332, USA*
[92] *IGFAE, Campus Sur, Universidade de Santiago de Compostela, 15782 Spain*
[93] *The Chinese University of Hong Kong, Shatin, NT, Hong Kong*
[94] *Stony Brook University, Stony Brook, NY 11794, USA*
[95] *Center for Computational Astrophysics, Flatiron Institute, New York, NY 10010, USA*
[96] *NASA Goddard Space Flight Center, Greenbelt, MD 20771, USA*

[97] *Dipartimento di Fisica, Università degli Studi di Genova, I-16146 Genova, Italy*
[98] *Institute for Gravitational and Subatomic Physics (GRASP), Utrecht University, Princetonplein 1, 3584 CC Utrecht, Netherlands*
[99] *RESCEU, University of Tokyo, Tokyo, 113-0033, Japan.*
[100] *OzGrav, University of Melbourne, Parkville, Victoria 3010, Australia*
[101] *Università degli Studi di Sassari, I-07100 Sassari, Italy*
[102] *INFN, Laboratori Nazionali del Sud, I-95125 Catania, Italy*
[103] *Università di Roma Tor Vergata, I-00133 Roma, Italy*
[104] *INFN, Sezione di Roma Tor Vergata, I-00133 Roma, Italy*
[105] *University of Sannio at Benevento, I-82100 Benevento, Italy and INFN, Sezione di Napoli, I-80100 Napoli, Italy*
[106] *Villanova University, 800 Lancaster Ave, Villanova, PA 19085, USA*
[107] *Departamento de Astronomía y Astrofísica, Universitat de València, E-46100 Burjassot, València, Spain*
[108] *Universität Hamburg, D-22761 Hamburg, Germany*
[109] *Rochester Institute of Technology, Rochester, NY 14623, USA*
[110] *National Tsing Hua University, Hsinchu City, 30013 Taiwan, Republic of China*
[111] *OzGrav, Charles Sturt University, Wagga Wagga, New South Wales 2678, Australia*
[112] *CaRT, California Institute of Technology, Pasadena, CA 91125, USA*
[113] *Dipartimento di Ingegneria Industriale (DIIN), Università di Salerno, I-84084 Fisciano, Salerno, Italy*
[114] *Université Lyon, Université Claude Bernard Lyon 1, CNRS, IP2I Lyon / IN2P3, UMR 5822, F-69622 Villeurbanne, France*
[115] *Seoul National University, Seoul 08826, Republic of Korea*
[116] *Pusan National University, Busan 46241, Republic of Korea*
[117] *INAF, Osservatorio Astronomico di Padova, I-35122 Padova, Italy*
[118] *University of Arizona, Tucson, AZ 85721, USA*
[119] *Rutherford Appleton Laboratory, Didcot OX11 0DE, United Kingdom*
[120] *OzGrav, Swinburne University of Technology, Hawthorn VIC 3122, Australia*
[121] *Université libre de Bruxelles, Avenue Franklin Roosevelt 50 - 1050 Bruxelles, Belgium*
[122] *Universitat de les Illes Balears, IAC3—IEEC, E-07122 Palma de Mallorca, Spain*
[123] *Université Libre de Bruxelles, Brussels 1050, Belgium*
[124] *Departamento de Matemáticas, Universitat de València, E-46100 Burjassot, València, Spain*
[125] *Texas Tech University, Lubbock, TX 79409, USA*
[126] *The Pennsylvania State University, University Park, PA 16802, USA*
[127] *University of Rhode Island, Kingston, RI 02881, USA*
[128] *The University of Texas Rio Grande Valley, Brownsville, TX 78520, USA*
[129] *Bellevue College, Bellevue, WA 98007, USA*
[130] *Scuola Normale Superiore, Piazza dei Cavalieri, 7 - 56126 Pisa, Italy*
[131] *MTA-ELTE Astrophysics Research Group, Institute of Physics, Eötvös University, Budapest 1117, Hungary*
[132] *Maastricht University, P.O. Box 616, 6200 MD Maastricht, Netherlands*
[133] *University of Portsmouth, Portsmouth, PO1 3FX, United Kingdom*
[134] *The University of Sheffield, Sheffield S10 2TN, United Kingdom*
[135] *Université Lyon, Université Claude Bernard Lyon 1, CNRS, Laboratoire des Matériaux Avancés (LMA), IP2I Lyon / IN2P3, UMR 5822, F-69622 Villeurbanne, France*
[136] *Dipartimento di Scienze Matematiche, Fisiche e Informatiche, Università di Parma, I-43124 Parma, Italy*
[137] *INFN, Sezione di Milano Bicocca, Gruppo Collegato di Parma, I-43124 Parma, Italy*
[138] *Physik-Institut, University of Zurich, Winterthurerstrasse 190, 8057 Zurich, Switzerland*
[139] *University of Chicago, Chicago, IL 60637, USA*
[140] *Université de Strasbourg, CNRS, IPHC UMR 7178, F-67000 Strasbourg, France*
[141] *West Virginia University, Morgantown, WV 26506, USA*
[142] *Montclair State University, Montclair, NJ 07043, USA*
[143] *Colorado State University, Fort Collins, CO 80523, USA*
[144] *Institute for Nuclear Research, Hungarian Academy of Sciences, Bem t'er 18/c, H-4026 Debrecen, Hungary*
[145] *Department of Physics, University of Texas, Austin, TX 78712, USA*
[146] *CNR-SPIN, c/o Università di Salerno, I-84084 Fisciano, Salerno, Italy*
[147] *Scuola di Ingegneria, Università della Basilicata, I-85100 Potenza, Italy*
[148] *Gravitational Wave Science Project, National Astronomical Observatory of Japan (NAOJ), Mitaka City, Tokyo 181-8588, Japan*
[149] *Observatori Astronòmic, Universitat de València, E-46980 Paterna, València, Spain*
[150] *The University of Utah, Salt Lake City, UT 84112, USA*
[151] *Kenyon College, Gambier, OH 43022, USA*
[152] *Vrije Universiteit Amsterdam, 1081 HV, Amsterdam, Netherlands*
[153] *University of Szeged, Dóm tér 9, Szeged 6720, Hungary*

[154] *Universiteit Gent, B-9000 Gent, Belgium*
[155] *Cornell University, Ithaca, NY 14850, USA*
[156] *University of British Columbia, Vancouver, BC V6T 1Z4, Canada*
[157] *Tata Institute of Fundamental Research, Mumbai 400005, India*
[158] *INAF, Osservatorio Astronomico di Capodimonte, I-80131 Napoli, Italy*
[159] *The University of Mississippi, University, MS 38677, USA*
[160] *University of Michigan, Ann Arbor, MI 48109, USA*
[161] *Texas A&M University, College Station, TX 77843, USA*
[162] *Dipartimento di Fisica, Università di Trieste, I-34127 Trieste, Italy*
[163] *American University, Washington, D.C. 20016, USA*
[164] *Carleton College, Northfield, MN 55057, USA*
[165] *University of California, Berkeley, CA 94720, USA*
[166] *Maastricht University, 6200 MD, Maastricht, Netherlands*
[167] *Directorate of Construction, Services & Estate Management, Mumbai 400094, India*
[168] *Vanderbilt University, Nashville, TN 37235, USA*
[169] *Universiteit Antwerpen, Prinsstraat 13, 2000 Antwerpen, Belgium*
[170] *University of Białystok, 15-424 Białystok, Poland*
[171] *University of Southampton, Southampton SO17 1BJ, United Kingdom*
[172] *Chung-Ang University, Seoul 06974, Republic of Korea*
[173] *Institut de Física d'Altes Energies (IFAE), Barcelona Institute of Science and Technology, and ICREA, E-08193 Barcelona, Spain*
[174] *University of Washington Bothell, Bothell, WA 98011, USA*
[175] *Institute of Applied Physics, Nizhny Novgorod, 603950, Russia*
[176] *Ewha Womans University, Seoul 03760, Republic of Korea*
[177] *Inje University Gimhae, South Gyeongsang 50834, Republic of Korea*
[178] *Korea Astronomy and Space Science Institute, Daejeon 34055, Republic of Korea*
[179] *National Institute for Mathematical Sciences, Daejeon 34047, Republic of Korea*
[180] *Ulsan National Institute of Science and Technology, Ulsan 44919, Republic of Korea*
[181] *Bard College, 30 Campus Rd, Annandale-On-Hudson, NY 12504, USA*
[182] *Institute of Mathematics, Polish Academy of Sciences, 00656 Warsaw, Poland*
[183] *National Center for Nuclear Research, 05-400 Świerk-Otwock, Poland*
[184] *Université de Montréal/Polytechnique, Montreal, Quebec H3T 1J4, Canada*
[185] *Laboratoire Lagrange, Université Côte d'Azur, Observatoire Côte d'Azur, CNRS, F-06304 Nice, France*
[186] *Sungkyunkwan University, Seoul 03063, Republic of Korea*
[187] *NAVIER, École des Ponts, Univ Gustave Eiffel, CNRS, Marne-la-Vallée, France*
[188] *Institute for High-Energy Physics, University of Amsterdam, Science Park 904, 1098 XH Amsterdam, Netherlands*
[189] *NASA Marshall Space Flight Center, Huntsville, AL 35811, USA*
[190] *University of Washington, Seattle, WA 98195, USA*
[191] *Dipartimento di Matematica e Fisica, Università degli Studi Roma Tre, I-00146 Roma, Italy*
[192] *INFN, Sezione di Roma Tre, I-00146 Roma, Italy*
[193] *ESPCI, CNRS, F-75005 Paris, France*
[194] *Concordia University Wisconsin, Mequon, WI 53097, USA*
[195] *Università di Camerino, Dipartimento di Fisica, I-62032 Camerino, Italy*
[196] *School of Physics Science and Engineering, Tongji University, Shanghai 200092, China*
[197] *Southern University and A&M College, Baton Rouge, LA 70813, USA*
[198] *Centre Scientifique de Monaco, 8 quai Antoine Ier, MC-98000, Monaco*
[199] *Indian Institute of Technology Madras, Chennai 600036, India*
[200] *Saha Institute of Nuclear Physics, Bidhannagar, West Bengal 700064, India*
[201] *Institut des Hautes Etudes Scientifiques, F-91440 Bures-sur-Yvette, France*
[202] *Indian Institute of Science Education and Research, Kolkata, Mohanpur, West Bengal 741252, India*
[203] *Department of Astrophysics/IMAPP, Radboud University Nijmegen, P.O. Box 9010, 6500 GL Nijmegen, Netherlands*
[204] *Consiglio Nazionale delle Ricerche - Istituto dei Sistemi Complessi, Piazzale Aldo Moro 5, I-00185 Roma, Italy*
[205] *Hobart and William Smith Colleges, Geneva, NY 14456, USA*
[206] *International Institute of Physics, Universidade Federal do Rio Grande do Norte, Natal RN 59078-970, Brazil*
[207] *Museo Storico della Fisica e Centro Studi e Ricerche "Enrico Fermi", I-00184 Roma, Italy*
[208] *Lancaster University, Lancaster LA1 4YW, United Kingdom*
[209] *Università di Trento, Dipartimento di Matematica, I-38123 Povo, Trento, Italy*
[210] *Indian Institute of Science Education and Research, Pune, Maharashtra 411008, India*
[211] *Dipartimento di Fisica, Università degli Studi di Torino, I-10125 Torino, Italy*
[212] *Indian Institute of Technology, Palaj, Gandhinagar, Gujarat 382355, India*

[213] *Departamento de Matemática da Universidade de Aveiro and Centre for Research and Development in Mathematics and Applications, Campus de Santiago, 3810-183 Aveiro, Portugal*
[214] *Marquette University, 11420 W. Clybourn St., Milwaukee, WI 53233, USA*
[215] *Università di Firenze, Sesto Fiorentino I-50019, Italy*
[216] *INAF, Osservatorio Astrofisico di Arcetri, Largo E. Fermi 5, I-50125 Firenze, Italy*
[217] *Indian Institute of Technology Hyderabad, Sangareddy, Khandi, Telangana 502285, India*
[218] *INAF, Osservatorio di Astrofisica e Scienza dello Spazio, I-40129 Bologna, Italy*
[219] *Andrews University, Berrien Springs, MI 49104, USA*
[220] *Dipartimento di Scienze Aziendali - Management and Innovation Systems (DISA-MIS), Università di Salerno, I-84084 Fisciano, Salerno, Italy*
[221] *Van Swinderen Institute for Particle Physics and Gravity, University of Groningen, Nijenborgh 4, 9747 AG Groningen, Netherlands*
[222] *Vrije Universiteit Brussel, Boulevard de la Plaine 2, 1050 Ixelles, Belgium*
[223] *Vrije Universiteit Amsterdam, 1081 HV Amsterdam, Netherlands*
(compiled March 21, 2022)

[a] Deceased, August 2020.